Title:

Cellular mechanisms underlying beneficial versus detrimental effects of bacterial antitumor immunotherapy

Authors:

Jesse Garcia Castillo[1,3], Sebastian Fernandez[2,3], Timothy Campbell[1], Jacob Williams[1], Diego Gonzalez-Ventura[1], Julia Ybarra[1], Nicole Flores Hernandez[1], Elina Wells[1], Daniel A. Portnoy[1,2], and Michel DuPage[1]

Affiliations:

[1] Division of Immunology and Molecular Medicine, Department of Molecular and Cell Biology, University of California, Berkeley, Berkeley, CA 94720, USA

[2] Department of Plant and Microbiology, University of California, Berkeley, Berkeley, CA 94720, USA

[3] These authors contributed equally

Contact info: dupage@berkeley.edu

Summary:

Listeria monocytogenes engineered to express tumor antigens as a cancer vaccine has yielded mixed results. Here, we utilized an attenuated strain of *Listeria* (*ΔactA, Lm*) that does not express tumor antigen to explore the immunological response to *Listeria* itself in the context of intravenous (IV), intratumoral (IT), or a combination of IV+IT administration into tumor-bearing mice. Unexpectedly, we found that *Lm* persisted in tumors of immune competent mice, regardless of the administration route. While IT *Lm* alone led to the recruitment of immunosuppressive immune cells that promoted tumor growth, IV *Lm* followed by IT *Lm* controlled tumor growth. IV *Lm* vaccination generated a pool of anti-*Lm* cytotoxic CD8 T cells that killed *Lm*-infected non-tumor cells to control tumor growth. Our findings reveal a differential impact of IT *Lm* administration on tumor progression that depends on the presence of anti-*Lm* CD8 T cells, rather than antitumor CD8 T cells, for antitumor therapeutic efficacy.

Introduction:

At the turn of the 20th century, William Coley was the first to demonstrate the efficacy and application of bacterial cancer immunotherapies through combinations of intratumoral and systemic injections of cultured bacteria (gram-positive *Streptococci* and gram-negative *Serratia*) into patients with bone and soft-tissue sarcomas[1–3]. Today, direct intravesical administration of Bacillus Calmette-Guerin (BCG), a live attenuated

strain of the gram-positive intracellular pathogen *Mycobacterium bovis*, is a standard of care for non-muscle-invading bladder cancer and the only FDA approved remnant of bacterial cancer therapy[4]. Recently, the discovery that bacteria naturally colonize many solid tumors has uncovered the potential of bacteria to serve as a drug delivery system or even as a cancer detection probe[5–14] . Improved methods to genetically manipulate bacterial genomes has also made it feasible to engineer bacteria that express tumor antigens, cytokines or cytotoxic proteins to control cancer[15–18]. Hence, multiple breakthroughs in manipulating bacteria and their activity in the tumor microenvironment has reignited interest in the potential for effective bacterial-based cancer immunotherapies.

Listeria monocytogenes engineered to express tumor-associated antigens and injected intravenously has effectively controlled multiple cancer models in mice[19–23]. To date, *Listeria* engineered to express tumor antigens and injected intravenously is the most tested bacterial-based immunotherapy in clinical trials for cancer[24]. Despite strong evidence of the vaccine's capacity to safely generate tumor antigen-specific CD8 T cells, the anti-cancer efficacy in patients has been mixed[25–30]. While select trials have shown improved outcomes in patients with otherwise untreatable cancers, such as malignant pleural mesothelioma or cervical cancer[25,27], many *Listeria*-based vaccine trials have not shown significant improvement in tumor control compared to standards of care. Therefore, it is critically important to discern why these vaccines fail despite generating antitumor CD8 T cells. In contrast to other bacterial cancer therapies, whether *Listeria* directly colonizes tumors has not been adequately investigated, likely because colonization was never a goal for its use against cancer in patients. A better understanding of the dynamics of *Listeria* interaction with host immune cells, its migration, and its persistence in tissues may reveal vulnerabilities of the current *Listeria*-based strategies as well as lead to improved uses of *Listeria* as an immune adjuvant directly within tumors.

Effective antitumor immunity requires a robust pool of antitumor immune cells and a permissive tumor microenvironment (TME) that allows for antitumor immune cells to function[15,31–33]. However, the TME is often highly immunosuppressive, allowing cancer cells to evade the immune system despite the presence of tumor-specific cytotoxic CD8 T cells[34,35]. Thus, the failure of *Listeria* vaccines might be due to *Listeria's* singular use as a systemic therapy to generate antitumor CD8 T cells, without harnessing its capacity to stimulate the innate arm of the immune system and reverse immunosuppression directly within tumors. *Listeria* is rich in mechanisms to stimulate innate immunity directly in tumors[36]. Direct intratumoral injection of bacteria or bacterial products may have underlied the success of William Coley's early therapies[37]. Recent preclinical studies as well as clinical trials have demonstrated the feasibility and efficacy of direct intratumoral injection of immune adjuvants naturally generated by *Listeria* and other bacterial species that can activate host cell pattern recognition receptors (PRRs)

and stimulate the innate immune response against tumors[38–40]. Direct IT injection of TLR1/2 agonists or cyclic dinucleotides (CDNs) was shown to increase CD8 T cell infiltration, polarize tumor-associated macrophages (TAMs) toward an inflammatory M1 anti-tumor phenotype, and synergize with checkpoint blockade therapy to control multiple tumor types in mice[40–44]. Thus, PRR agonists injected directly into tumors can drive potent antitumor immunity without necessitating tumor antigen vaccination. However, a better understanding of *Listeria*'s impact on the TME and the landscape of immune cells is needed before mechanisms to synergize the innate and adaptive immune-activating capacities of *Listeria* can be translated into a more effective treatment of cancer.

Here, we show that either intratumoral (IT) or intravenous (IV) injection of *ΔactA*-attenuated *Listeria* (*Lm*) that is not engineered to express tumor antigens did not control tumor growth. Instead, IT *Lm* promoted tumor progression and *Lm* persisted predominantly in polymorphonuclear cells (PMNs) within the TME. *Lm* persistence in tumors was the result of IT *Lm* recruiting PMNs into the TME where they were polarized into a myeloid-derived suppressor cell phenotype (PMN-MDSC) that could suppress antitumor CD8 T cells[42,43]. In contrast, prior vaccination of mice against *Lm* by IV injection, either early in tumor development or prior to tumor initiation, led to strong tumor control upon IT *Lm* administration, even against highly aggressive sarcomas from genetically engineered mice. Tumor control required perforin-mediated killing by CD8 T cells specific to *Lm* antigen, which could eliminate PMN-MDSCs harboring *Lm* within the TME. Killing of *Lm*-infected host cells mediated significant tumor control without the direct killing of tumor cells by tumor-specific or *Listeria*-specific CD8 T cells. Altogether, these results show that generating a strong, localized anti-bacterial CD8 T cell response in tumors is sufficient to overcome the suppressive TME and inhibit tumor growth. Importantly, this work redefines the goals for effective anti-cancer bacterial therapies by revealing a critical role for direct T cell targeting of conserved bacterial antigens, which is more broadly applicable and rapidly translatable compared to engineering bacteria to express patient-tailored tumor-specific neoantigens. These findings are fundamental to developing better *Listeria*-based cancer therapies.

Results

Intratumoral injection of attenuated *Listeria* increases tumor growth.

Immune adjuvants (i.e. PRR agonists) alone are effective against cancers when delivered directly into tumors without the addition of engineered tumor antigens[38,44] . To test whether antitumor responses could be generated by direct intratumoral (IT) injection of an attenuated strain of *L. monocytogenes*, which is not engineered to express tumor-specific antigens, we used an *ΔactA* mutant, denoted *Lm*, which contains the primary attenuating mutation used in many *Listeria* vaccine trials in patients[45]. *ΔactA*

Listeria lack the ActA virulence factor, making the bacteria unable to polymerize host actin and spread from cell to cell, but importantly, *Lm* can still escape from phagosomes and grow in the host cell cytosol, making it a potent inducer of MHC-I-restricted CD8 T cell responses. The *ΔactA* mutation renders *Lm* 1,000-10,000-fold less virulent than WT *L. monocytogenes* without decreasing its capacity to induce CD8 T cells[46]. This feature has led to its use in many *Listeria*-based clinical trials due to its increased safety in patients[25,26,28,29]. However, the direct injection of *Listeria* into tumors of cancer patients has never been tested. We performed dose-escalating experiments with IT *Lm*, from $5x10^5$-$5x10^7$ CFUs, into tumors 11 days post tumor inoculation, when tumors just became palpable, and found no lethality at a dose of $5x10^7$ *Lm*. Therefore, we used $5x10^7$ CFUs for IT *Lm* injections throughout subsequent experiments. IT injection of *Lm* did not result in tumor control in either MC38 or B16F10 tumor models but instead led to a significant increase in tumor growth **(Figures 1A-1C).** This result was unexpected, as *Lm* has been widely tested in experimental mouse models and was not observed to cause increased tumor growth. However, IT injection of *Lm* was never tested, so we hypothesized that this route of administration might be responsible for increased tumor growth. Therefore, we tested the impact of *Lm* administration on tumor growth after intravenous (IV) delivery, the most commonly used method of administration, of $1x10^6$ *Lm* (a lower dose was required to prevent lethality by an IV route)[19]. In this scenario, we found no increase in tumor growth of B16F10 or MC38 tumors, nor did we observe tumor growth control using the *Lm* strain **(Figures S1A-1C)**. This finding is significant, as the route of *Lm* inoculation, IT versus IV, appears to convert *Lm* from either being detrimental or potentially therapeutic for the control of cancer.

***Lm* colonizes tumors and persists in immunocompetent mice.**

We hypothesized that the varying impacts on tumor growth after IT compared to IV *Lm* routes of administration could be due to varying *Lm* colonization in lymphoid organs or the tumor itself. To examine the localization of *Lm* in tumor-bearing mice after IV or IT *Lm* administration, we measured colony forming units (CFUs) for living bacteria from various tissues harvested from tumor-bearing mice at several time points after *Lm* administration. We found that *Lm* was cleared from spleens, lymph nodes, and liver by 5-10 days post injection in tumor-bearing mice, regardless of the route of delivery **(Figures 1D-E)**. However, while *Lm* numbers peaked at 10^5-10^6 CFU in the spleen and liver shortly after IV injection, *Lm* CFUs were much lower in these organs after IT injection, despite a 50-fold greater number of bacteria administered in IT-injected mice. These results confirm that the different routes of *Lm* administration and different doses of *Lm* injected lead to a different biodistribution of *Lm* in mice. Nevertheless, *Lm* injected either IV or IT colonized both tumor models for up to 15 days, when experiments were ended due to uncontrolled tumor growth **(Figures 1D-E, and S1D)**. The persistence of live *Lm* within tumors long-term (more than 3-5 days) in immunocompetent mice has not

been documented. Furthermore, the colonization and persistence of *Lm* in tumors after IV administration revealed that systemic routes of *Lm* administration can lead to seeding, growth, and long-term colonization of *Lm* in tumors, making *Lm* deliverable to tumors that are not easily accessible for direct IT injection. However, whereas IV leads to an increased early exposure of *Lm* to lymphoid tissues, IT injection leads to a greater bacterial load early within tumors, potentially impacting the antitumor immune response.

***Lm* infects PMN-MDSCs in tumors.**

We hypothesized that the distribution of *Lm* in specific cells of the tumor microenvironment after IT administration shaped the immune response to promote tumor growth. Because *Lm* is a facultative intracellular pathogen which primarily resides in host cells after infection, we sought to identify which cells harbor bacteria in the tumors of *Lm*-treated mice. To monitor intracellular infection of host cells by *Lm*, we used a fluorescent-protein based system wherein a Tag-RFP reporter was expressed under the control of the *actA* promoter in *ΔactA Listeria*, denoted *Lm-RFP* **(Figure 2A)**[47]. Since the *actA* promoter is induced more than 100-fold *when Lm* enters the host cell cytosol, expression of Tag-RFP indicates that the bacteria have entered the cytosol of a cell[48]. We observed co-localization of the RFP signal exclusively in $CD45^+$ immune cells from single cell suspensions of MC38 or B16F10 tumors infected with *Lm-RFP*. Notably, we did not observe RFP fluorescence in $CD45^-$ cells, which includes tumor cells (**Figure 2B**).

Next, we tracked which types of $CD45^+$ immune cells harbored *Lm* in their cytosol. At 4-and 24-hours post-infection, we observed an enrichment of RFP-expressing bacteria in phagocytic immune cells, especially $Ly6G^+$ polymorphonuclear (PMN) cells (**Figures 2C and S2A-D**)**.** To a lesser extent, *Lm-RFP* was detected in $F4/80^+$ macrophages, $Ly6C^+$ monocytes, and $CD11c^+MHC\text{-}II^+$ dendritic cells (**Figures 2C and S2B**). This distribution of *Lm* in phagocytic immune cells, primarily PMNs and macrophages, was maintained after the initial infection for up to five days (**Figure 2D**). However, in comparison to tumors at steady state, IT *Lm* only induced a significant influx of PMNs into tumors, whereas other phagocytic cell frequencies were unchanged (**Figures 2E and S2C-E)**. The RFP^+ PMNs also increased between 4 and 24 hours after IT delivery (**Figure 2F**). Altogether, these results demonstrated that PMNs are the primary reservoir for *Lm* in the TME. This result was unanticipated, as we expected PMNs would rapidly kill phagocytosed *Lm*, preventing their escape into the cytosol and the expression of RFP[49–51].

We hypothesized that the escape of *Lm* into the cytosol of PMNs and the long term colonization of *Lm* in the TME was the result of PMN conversion into PMN-MDSCs[52,53]. Myeloid cells, including PMNs, have been shown to differentiate into myeloid derived suppressor cells (MDSCs) in tumors, which have the capacity to promote tumor development and metastasis by inhibiting T cell responses against tumor

cells[32,54]. MDSCs are identified as a population of $CD45^+$ immune cells that stain positively with anti-CD11b and anti-Gr-1 antibodies[32]. The anti-Gr-1 antibody is dually reactive to Ly6G and Ly6C, and by using antibodies to each of these specific proteins, two populations of MDSCs, monocytic (M-MDSCs) and granulocytic (G- or PMN-MDSCs), respectively, have been described[55–57]. Markers to distinguish suppressive PMN-MDSCs from their non-suppressive PMN counterparts have been well-characterized, e.g. expression of CD14, PD-L1, Arg1, and CD300ld are associated with a MDSC phenotype[55–58]. Phenotyping of PMNs between 4 and 24 hours after IT *Lm* revealed a dynamic increase in PMNs expressing the prototypical PMN-MDSC marker CD14, with more than 90% of PMNs expressing CD14 by 24 hours after IT *Lm* in MC38 tumors (**Figures 2G and S2G)**. Interestingly, *Lm* localized preferentially in the $CD14^+$ PMN-MDSCs as compared to $CD14^-$ PMNs (**Figure 2H**). In B16F10 tumors, *Lm* was also found almost exclusively in $CD14^+$ PMN-MDSCs, revealing a strong selectivity for *Lm* in the cytosol of PMN-MDSCs in two tumor models (**Figure S2E-H**). These results fit a scenario in which PMNs recruited by *Lm* to tumors rapidly adopt a MDSC phenotype and become a reservoir for *Lm* colonization of their cytosol.

IT *Lm* recruits PMNs that differentiate into pro-tumorigenic PMN-MDSCs within the tumor microenvironment.

We hypothesized that PMNs become permissive to *Lm* escape into and growth in the cytosol due to their differentiation into an immunosuppressive cell type in the TME. To test this, we used conditionally immortalized neutrophils (CINs) or primary bone marrow progenitors differentiated into PMNs *in vitro* (**Figures 3A and S3A**)[59,60]. PMNs cultured in supernatants from MC38 or B16F10 tumor cells increased their expression of the PMN-MDSC markers CD14 and PD-L1 (**Figures 3B**). As a positive control, PMNs were differentiated into PMN-MDSCs by adding IL-6 and GM-CSF, which led to a similar induction of CD14 and PD-L1 in CINs and bone marrow derived PMNs[59]. To evaluate whether the adoption of the MDSC phenotype was associated with increased susceptibility to *Lm* infection, we infected these heterogeneous cells *in vitro* with *Lm-RFP* and monitored infection by flow cytometry. The $CD14^+$ PMNs were almost exclusively associated with *Lm* cytosolic infection as determined by RFP expression (**Figures 3C and S3B**). These results strongly suggest that IT *Lm* recruits PMNs to tumors where they become converted into PMN-MDSCs that allow for *Lm* to infect and persist intracellularly in PMN-MDSCs.

PMN-MDSCs are widely associated with decreased antitumor immunity and increased tumor progression. Therefore, we hypothesized that *Lm*-mediated recruitment of PMNs and their conversion into PMN-MDSCs may underlie the increased tumor growth observed after IT *Lm*. To test this hypothesis, we depleted PMNs prior to tumor development using anti-Ly6G antibodies (**Figure 3D**). In this setting, IT *Lm* no longer increased tumor growth, whereas in mice without *Lm*, anti-Ly6G had no effect on tumor

growth, indicating that the increased tumor progression after IT *Lm* required Ly6G$^+$ PMNs **(Figure 3E)**. However, PMN depletion did not reduce bacterial colonization in tumors as measured by CFU analysis (**Figure S3C**). Using *Lm-RFP*, we found *Lm* was present primarily in macrophages, whose frequency was unchanged by IT *Lm* and whose infection with *Lm* did not increase tumor growth (**Figures S3D-E**). These results showed that IT *Lm* recruits PMNs to tumors where they are converted to an MDSC phenotype that promotes increased tumor growth. MDSCs have been shown to promote tumor growth by inhibiting antitumor CD8 T cell responses[32,54]. To test this, we co-cultured tumor-specific CD8$^+$ T cells (*in vitro* activated OT-I T cells) with OVA-expressing MC38 tumor cells in the presence or absence of PMN-MDSCs isolated from MC38 tumors 24 hours after IT *Lm*. The addition of PMN-MDSCs led to a significant reduction in IFNγ cytokine production from OT-I T cells in response to direct recognition of OVA-expressing tumors (**Figure 3F-G**). Therefore, *Lm* injection into tumors can promote tumor growth by recruiting PMNs that differentiate into PMN-MDSCs that can suppress antitumor-specific CD8 T cells.

A combination of IV+IT *Lm* leads to tumor control across multiple cancer models.

As neither IV nor IT administration of *Lm* alone provided strong tumor control, we considered that both routes of infection together might generate therapeutic efficacy. We reasoned that IV injection of *Lm* would effectively generate adaptive T cell responses against *Lm*[61], and that subsequent IT *Lm* injection would then recruit anti-*Lm* T cells into tumors to augment the antitumor immune response. To test this hypothesis, we inoculated mice with MC38 or B16F10 tumors and administered *Lm* IV four days later. At 11 days after tumor inoculation, when tumors were palpable, we injected *Lm* IT into tumors as done previously with IT *Lm* alone **(Figure 4A)**. This combination of IV *Lm* followed by IT *Lm* administration now significantly controlled both MC38 and B16F10 tumors **(Figures 4B-C)**. Importantly, tumor control occurred without the use of a *Lm* strain that expressed any tumor antigens. Tumor control was evident by 9 days after IT *Lm* injection, and tumors remained controlled throughout the experiment. Overall, of the experiments performed, only IV+IT Lm administration led to tumor rejection (20% of mice, 8 out of 40) and tumor rejection was never observed with IV or IT alone. In addition, we found that while Ly6G$^+$ PMNs were recruited equally to tumors 24 hours after IT *Lm* administration in both the IV+IT and IT-only dosing regimens, the frequency of Ly6G$^+$ cells were significantly reduced by 5 days after IT *Lm* administration in the IV+IT setting **(Figure 4D)**. Furthermore, the fraction of CD14$^+$ PMNs was almost completely abolished 5 days after IT *Lm* administration in the IV+IT *Lm* dosing regimen, a reduction even below their frequency in PBS-treated control tumors despite their robust increase 24 hours after IT *Lm* **(Figure 4E)**. Finally, when we depleted PMNs prior to tumor inoculation and then used the IV+IT *Lm* regimen, we did not observe any enhancement in tumor control, indicating that the PMN reductions with IV+IT *Lm* are

sufficient to prevent PMN-MDSC promotion of tumor growth after the IT *Lm* dose in the IV+IT therapeutic regimen **(Figure S4A)**.

Next, we wanted to establish whether *Lm* persisted in tumors in the setting of IV+IT *Lm* administration. While *Lm* persisted in approximately 80% of tumors up to 10 days after IT *Lm* administration, *Lm* was ultimately cleared from tumors, with CFUs dropping to below the level of detection between days 15-20 after IT *Lm* (day 21-30 of tumor growth) **(Figure 4F)**. We hypothesized that the clearance of *Lm* from tumors was the result of *Lm*-specific T cells that were generated by IV *Lm* and then recruited to tumors when *Lm* was injected IT. Therefore, tumor control with the IV+IT *Lm* dosing could be the result of the recruitment of *Lm*-specific T cells to tumors. Alternatively, because *Lm* entered and propagated within the TME after IV administration at day 4 (**Figure S1D**), the early seeding of tumors might contribute to tumor control by changing the TME to augment the second IT injection of *Lm* in the IV+IT regimen. To address this possibility, we performed experiments in which IV *Lm* was administered prophylactically, 20 days prior to tumor inoculation (**Figure 4G**). In this setting, *Lm* was completely cleared from mice prior to tumor inoculation and therefore absent from tumors when IT *Lm* was administered. Now we could test whether recalled *Lm*-specific adaptive immune cells, rather than changes in the distribution or amount of *Lm* in tumors, was responsible for the antitumor efficacy of the IV+IT regimen. This experiment showed clearly that mice injected with *Lm* prophylactically (memory IV+IT) controlled tumors equivalently to our standard IV+IT regimen **(Figure 4H)**. However, prophylactic IV *Lm* injection alone, or IV *Lm* followed by a subcutaneous injection of *Lm* on the contralateral flank of mice (memory IV+SQ), did not control tumors **(Figure 4H)**. These results suggested that IT administration of *Lm* mediated antitumor immunity by recalling an adaptive immune response against *Lm* locally within the tumor.

Finally, we tested the IV+IT *Lm* dosing regimen in a clinically relevant mouse sarcoma model - the tumor type most often treated by Coley, and a clinically relevant model amenable to direct IT injections[1,23,62]. Using an aggressive *Kras*$^{G12D/+}$*;p53*$^{fl/fl}$-generated orthotopic sarcoma model[63], we found that memory IV+IT *Lm* led to significant sarcoma control as well as *Lm* clearance from *Lm*-treated sarcomas compared to tumors treated with PBS that had received IV *Lm* prophylactically **(Figures 4I and S4C)**. Taken together, these results showed that IV+IT *Lm* can clear *Lm* from tumors and control tumor growth in a manner that is not recapitulated with IV or IT *Lm* administrations alone.

CD8 T cells are required for tumor control and *Lm* clearance with the IV+IT *Lm* dosing regimen.

The reduction of tumor growth that occurred during the IV+IT *Lm* treatment regimen compared to single-dose IV or IT *Lm* administrations suggested that an adaptive immune response mediated tumor control. We hypothesized that T cells were

the critical adaptive immune cells important for tumor control in the IV+IT dosing regimen due to their established role in both anti-*Lm* and antitumor immunity[61,64,65]. Indeed, flow cytometric analysis of tumors 5-8 days after IT *Lm* injection revealed an increase in the frequencies of both intratumoral CD8 and CD4 T cells in mice receiving IV+IT *Lm* compared to IV-only or IT-only *Lm* injections or PBS control injections (**Figures 5A-C, S5A-B**). Examination of tumors at the endpoint of tumor growth (15-20 days after IT *Lm* injection) also revealed a significant increase in the infiltration of CD8 T cells, but not a significant increase in CD4 T cells, in tumors of mice treated with IV+IT *Lm* compared to other groups (**Figures 5A-C, S5A-B**). Intratumoral regulatory T cells (Tregs) that are known to be immunosuppressive in the TME, were not significantly reduced with the IV+IT regimen compared to IV or IT alone, although they were reduced compared to the PBS treated mice (**Figures S5C-D**)[15,31–33,66–68]. Next, we assessed the functionality of the CD8 T cells by IFNγ and TNFα production 8 days after IT *Lm* or PBS injection. Here, the IV+IT *Lm* dosing regimen significantly increased CD8 T cells production of IFNγ, but especially the dual production of IFNγ and TNFα compared to PBS, IT *Lm* only, or IV *Lm* only (**Figure 5D**).

To test whether $CD4^+$, $CD8^+$, or both populations of T cells were required for tumor control, we used antibody-mediated depletion of the T cells beginning one day prior to IT *Lm* injection **(Figure 5E)**. Depletion of CD8 T cells, but not CD4 T cells, abrogated the efficacy of the IV+IT *Lm* regimen, indicating that CD8 T cells were required for tumor control with IV+IT *Lm* **(Figure 5F)**. In addition, CD8 T cell depletion increased the frequency of $Ly6G^+$ cells maintained in tumors of mice treated with IV+IT *Lm*, suggesting that the reduction in PMN-MDSCs with IV+IT *Lm* is likely the result of CD8 T cell killing of *Lm*-infected PMNs (**Figure 5G**). We also tested the IV+IT dosing regimen in *Batf3*$^{-/-}$ mice that lack type I dendritic cells (DC1s), which are the primary DCs responsible for cross-presenting *Listeria* antigens to CD8 T cells[69,70]. The IV+IT dosing regimen did not lead to tumor control in *Batf3*$^{-/-}$ mice **(Figure 5H)**. Taken together, the above results suggested that IV+IT *Lm* therapy requires the activity of CD8 T cells. However, whether CD8 T cells specific to *Listeria*, the tumor, or both were required for tumor control could not be distinguished.

***Listeria*-specific CD8 T cells drive tumor control.**

To assess whether the CD8 T cells that mediate tumor control in response to IV+IT *Lm* treatment are specific to tumor or *Lm* antigens, we used MHC-I tetramers loaded with a tumor-derived or a *Lm*-derived peptide. We used *Lm* engineered to express ovalbumin (*Lm-OVA*) so that we could monitor SIINFEKL loaded H2-K^b tetramers to track the anti-*Lm* response (SIIN/H2K^b) (**Figure 6A, Figure S6A**). MuLV/H2K^b tetramers were used to track the tumor-specific response to an endogenous retrovirus that is reactivated in MC38 and B16F10 tumors (**Figure S6B**)[67,68]. Interestingly, there was a decrease in the frequency and number of tumor-

reactive CD8 T cells in mice receiving the IV+IT *Lm-OVA* compared to PBS treated mice (**Figure 6B**). However, both the number and frequency of anti-*Lm* CD8 T cells was significantly increased in the IV+IT regimen **(Figure 6C)**.

From these results, as well as the observation that IV+IT *Lm* led to a reduction in CFUs in tumors, we hypothesized that the anti-*Lm* CD8 T cell response may be essential for the efficacy of the IV+IT *Lm* regimen. While we did not find evidence of direct tumor cell infection by *Lm* using the *Lm-RFP* reporter strain **(Figures 2A-2D**), we sought to determine whether direct tumor cell killing by *Lm*-specific CD8 T cells was required for tumor control. To test this, we inoculated mice with MC38 tumors that did not express MHC-I (*B2m*$^{-/-}$) and therefore could not be directly recognized and killed by CD8 T cells targeting either *Lm* or tumor antigens. Even in this setting, IV+IT *Lm* promoted significant control of MHC-I-deficient MC38 tumors, indicating that tumor control does not require direct tumor cell recognition by CD8 T cells (**Figure 6D**).

To further test our hypothesis that the anti-*Lm* CD8 T cell response was sufficient for tumor control, we adoptively transferred activated T cell receptor (TCR) transgenic CD8 T cells from OT-I mice, which have a TCR that recognizes the OVA peptide SIINFEKL presented on MHC-I (SIIN/H2K^{b}), into mice prior to tumor inoculation. This strategy allowed for a pool of *Lm*(SIIN)-specific memory CD8 T cells to develop in recipient mice, analogous to the expansion of *Lm*-specific memory CD8 T cells in prophylactically IV *Lm*-treated mice (**Figure 4G-H**). When tumors became palpable at day 11, tumors were injected with PBS, *Lm*, or *Lm-OVA* (**Figure 6E**). Strikingly, only mice whose tumors were injected with *Lm-OVA* had delayed tumor growth, similar to mice that received a standard IV+IT *Lm* regimen (**Figure 6F**). Even in the aggressive orthotopic KP sarcoma model that does not express tumor-specific antigens[71], the transfer of *Lm*-specific CD8 T cells prior to tumor implantation and IT *Lm-OVA* treatment was sufficient to provide significant tumor control (**Figure 6G**). These results indicate that a CD8 T cell response specific to *Lm* antigens is sufficient to phenocopy the effect of IV *Lm* in the IV+IT *Lm* dosing regimen.

We hypothesized that the *Lm*-specific CD8 T cells were able to mediate tumor control in the context of tumor-reactive CD8 T cells that were augmented by the activity of the anti-*Lm* CD8 T cell response. However, to test whether the anti-*Lm* CD8 T cells alone were able to mediate tumor control, we injected *in vitro* activated OT-I cells into *Rag2*-deficient mice, which lack T and B cells and therefore cannot mount an antitumor CD8 T cell response. We then implanted MC38 tumors and IT injected PBS, *Lm* or *Lm-OVA* at day 11 when tumors became palpable. Similar to our observation in wild-type mice, tumor growth was significantly reduced in *Rag-2*$^{-/-}$ mice that were IT injected with *Lm-OVA*, but not when injected with *Lm* that did not express OVA (**Figure 6H**). Thus, tumor control could be mediated directly by anti-*Lm* CD8 T cells in the TME even in the absence of tumor-specific CD8 T cells.

To test whether recognition of *Lm*-antigens on non-tumor cells infected with *Lm* was required for the efficacy of IV+IT *Lm*, we continued to use the transfer of OT-I CD8 T cells, but now into wildtype versus B2m-/- mice, which lack MHC-I on all host cells. Specifically, we inoculated wildtype MC38 versus MC38-*B2m*$^{-/-}$ tumor cells into wildtype versus *B2m*$^{-/-}$ mice that had OT-1 CD8 T cells transferred two weeks prior. In this scenario, we could determine whether tumor control with IV+IT *Lm* required the recognition of infected host cells or tumor cells directly by CD8 T cells. In the setting of wildtype MC38 tumors, MHC-I expression was required on host cells to mediate tumor control, as IT *Lm-OVA* was completely ineffective in *B2m*$^{-/-}$ mice despite the presence of OT-I T cells (**Figures 6I and S6C**). Furthermore, in the setting of MC38-*B2m*$^{-/-}$ tumors, OT-I T cells still mediated tumor control with IT *Lm-OVA*, but only in the setting of wildtype mice and not *B2m*$^{-/-}$ mice (**Figures 6I**). CFU analysis for live *Lm* also demonstrated that MHC-I expression on host cells, but not tumor cells, was absolutely required for *Lm* clearance from the TME (**Figure S6D**). Thus, CD8 T cells require MHC-I for TCR recognition of host cells, but not tumor cells to mediate tumor control and bacterial clearance in the IV+IT *Lm* regimen.

Finally, we wished to determine whether killing of non-tumor cells infected with *Lm* was required for the efficacy of IV+IT *Lm*, as tumor control could also be mediated by an alternative mechanism that requires other activities of *Lm*-specific CD8 T cells. We tested whether *Lm*-specific T cells required the pore-forming effector protein Perforin to mediate tumor control by adoptively transferring activated SIIN-specific CD8 T cells generated from WT mice or *Prf1*-deficient mice vaccinated with *Lm-OVA*. Mice were then inoculated with MC38 tumors, and at day 11 when tumors were palpable, tumors were IT injected with *Lm* or *Lm-OVA* **(Figure 6J-K)**. Tumor control was lost in mice that received *Prf1*$^{-/-}$ SIIN-specific CD8 T cells. The failure of *Prf1*$^{-/-}$ SIIN-specific CD8 T cells to mediate tumor control was not due to a failure of these cells to infiltrate the tumor, as an equivalent frequency of SIIN-specific CD8 T cells were found in tumors that received WT or *Prf1*$^{-/-}$ SIIN-specific CD8 T cells (**Figure S6E**). Taken together, these findings demonstrate that *Lm*-specific CD8 T cells that kill *Lm*-infected non-tumor cells are sufficient to mediate tumor control in the IV+IT *Lm* therapeutic treatment regimen.

Discussion:

In this study, we report two major findings. First, we showed that direct intratumoral injection of an attenuated strain of *Lm* causes increased tumor growth. This was due to *Lm*-mediated recruitment of PMNs that are converted within tumors to immunosuppressive MDSCs, which act as permissive cells for bacterial survival while suppressing antitumor CD8 T cells. Second, we showed that IT *Lm* tumor growth promotion could be converted to tumor control by prior IV *Lm* immunization, which generated anti-*Listeria* CD8 T cells whose activity alone could mediate cancer

protection. Thus, depending on the context of intratumoral seeding of *Lm* into a tumor, *Listeria* can either promote or inhibit cancer progression. These results reveal new insights into the biology of *Listeria* colonization of tumors in immune competent mice as well as the potential for anti-*Lm*-specific CD8 T cells to mediate cancer control. These findings should shape future approaches using *Listeria* as an anti-cancer therapeutic.

The *ΔactA* attenuated *Lm* strain used in this study selectively colonized and persisted in tumors when injected IT or IV. Other studies have also reported short-term persistence of bacteria in tumors, either growing intracellularly (e.g. *Salmonella*) and/or extracellularly (e.g. *Clostridium*, *Vibrio. cholerae*, *E. coli*), which in some cases had direct tumoricidal effects[5,72,73]. *Clostridium novyi* administered intravenously led to sporulation in the avascular regions of tumors that directly caused cancer cell death[13,74]. Longer term protection from cancer with *Clostridium* occurred in ~30% of mice and depended on the generation of CD8 T cells, though the specificity of the CD8 T cells, against bacteria or tumor, was never directly tested[13,74]. *E. coli* engineered to express α-hemolysin, a pore forming protein, or to deliver L-arginine to promote CD8 T cell function, both led to improved tumor control upon bacterial colonization of tumors[75,76].The prevalence of bacteria in tumors has been attributed to the presence of nutrients or an environment in tumors that is conducive to bacterial survival and growth[12,13,77–79]. *Salmonella typhimurium* engineered to infiltrate tumors by selective auxotrophy was effective at controlling several types of mouse tumors[12,77,80]. The lack of documentation of *Lm* persistence in tumors could be the result of using alternative attenuated strains of *Listeria,* or failing to look for *Lm* persistence in previous studies. However, in the case of *ΔactA*-attenuated *Listeria* colonization in this study, we hypothesize that bacterial migration via the bloodstream is stochastic, but upon arrival in tumors, *Listeria* is protected from immune clearance due to the immunosuppressive environment created in tumors that generates PMN-MDSCs that permit the intracellular growth of *Lm*[5,81].

PMN permissiveness for cytosolic *Lm* was strongly correlated with a $CD14^+$ and $PD\text{-}L1^+$ phenotype of the PMNs, markers associated with a MDSC phenotype. We also found that this phenotype was promoted by tumor derived factors, since culture of PMNs with tumor cell supernatants was sufficient to induce their expression of CD14 and PD-L1. In our system, however, depletion of these PMN-MDSCs did not prevent *Lm* persistence in tumors, but did prevent the accelerated tumor growth observed with IT *Lm* alone. This suggests that the TME prevents *Lm* clearance in multiple phagocytic immune cell types, but that recruitment and conversion of PMNs to MDSCs specifically

promotes cancer progression. PMN-MDSCs and other myeloid cells have been found to promote tumor growth by several mechanisms, such as inhibiting T cell responses as well as by promoting vasculature formation to support tumor cell proliferation in glioblastoma, pancreatic, and several other mouse tumor models[32,35,54]. Using *in vitro* co-culture of FACS-purified intratumoral PMN-MDSCs with tumor cells and antitumor CD8 T cells, we showed that PMN-MDSCs could inhibit cytokine production from CD8 T cells responding to antigen recognition on tumor cells. Altogether, we uncovered an unexpected consequence of *Lm* seeding and colonization of tumors, wherein bacterial colonization of tumors by *Lm* does not lead to direct tumoricidal effects, but rather, recruits immune cells that are subsequently converted into immunosuppressive cells that promote tumor growth. Furthermore, microbes have been shown to play a direct role in promoting immune tolerance, and so it is possible that *Lm* bacteria may also directly promote tolerance in the TME[82].

Attenuated *Listeria* vaccines generate memory CD8 and CD4 T cells that provide robust and long-lasting adaptive immunity[21,61]. We tested whether prior IV *Lm* administration to generate anti-*Lm* CD8 T cells would impact the immunosuppressive TME and promote tumor control with a secondary IT *Lm* dose. In this setting, IT *Lm* led to tumor control across multiple tumor models, including an aggressive orthotopic KP model of sarcoma. Tumor control was also observed if mice were prophylactically vaccinated prior to tumor inoculation, ruling out a role for tumor colonization with IV *Lm* in the efficacy of this IV+IT *Lm* regimen. Our results parallel previous approaches taking advantage of TDAP vaccination and using *Listeria* as a delivery system to introduce tetanus toxoid into tumors to elicit a $CD4^+$ memory T cell response to eliminate tumor cells[83]. However, in these reports, it was shown that the *Listeria* infected the cancer cells directly to drive T cell recognition and control of cancer[83]. However, using a TagRFP reporter of cytosolic *Lm*, we did not find evidence of direct infection of tumor cells. Nor was direct recognition of tumor cells by anti-*Lm* CD8 T cells required for tumor control, as MHC-I-deficient tumors were also controlled by the IV+IT *Lm* regimen. Differences in the attenuated strains of *Listeria* used in other studies compared to this study likely underlie these differences in tumor cell infiltration by bacteria. While our study uses an *ΔactA* mutation to attenuate the bacteria by preventing cell to cell spread, others have used attenuated *Listeria* that retains a functional *actA* gene, thus allowing for the spread of *Listeria* to non-phagocytic cells, including tumor cells[15–18,20,79,83,84].

To test the role of anti-*Lm*-specific CD8 T cells directly in tumor control with IT *Lm*, we used adoptively transferred OT-I CD8 T cells in place of IV *Lm* administration. We then used *Lm-OVA* IT delivery to show that OT-I T cells targeting only a surrogate *Lm* antigen (OVA), and incapable of recognizing tumor antigens, were able to mediate tumor control. Of note, in clinical trials using BCG treatment for bladder cancer, patients with a positive skin tuberculosis test (PPD) due to previous vaccination with BCG, responded better to the BCG treatment and had longer recurrence-free survival than

patients who did not establish pre-existing BCG-specific T cell immunity[85]. In our study, we ruled out that *Lm* directly infected cancer cells to mediate tumor control by showing that the IV+IT *Lm* regimen was effective in controlling MHC-I-deficient tumors that cannot be directly recognized by CD8 T cells. Furthermore, MHC-I-deficient tumors that did not express OVA were controlled by transfer of OT-I T cells followed by IT *Lm-OVA* delivery. However, MHC-I expression on non-tumor cells was essential for tumor control, as *B2m*-deficient mice receiving anti-*Lm* OT-I T cells were unable to control tumors after IT *Lm-OVA* administration. Therefore, CD8 T cell recognition of host cells, presumably $CD45^+$ immune cells that have taken up *Lm* in their cytosol, including PMN-MDSCs, was required for tumor control. Finally, we showed that anti-*Lm* CD8 T cells required killing of host cells, rather than the tumor cells directly, to mediate tumor control. Using prophylactic transfer of *Lm*(OVA)-specific CD8 T cells generated in *Prf1*$^{-/-}$ mice, we found that tumors were no longer controlled with IT *Lm-OVA* administration. These results are contrary to the established dogma that an increase in tumor-specific CD8 T cells is required for the efficacy of bacterial-based cancer immunotherapies[86]. These results also indicate that tumor control by CD8 T cells does not necessitate bacterial spread into tumor cells.

While further investigation of the mechanisms underlying tumor control in the IV+IT *Lm* regimen is needed, our results raise the tantalizing potential of a universal therapeutic vaccine for cancer[87]. The introduction of a microbe into a tumor may lead to tumor control if patients already have CD8 T cells targeting microbial antigens. Indeed, direct IT injection of an FDA-approved seasonal influenza vaccine demonstrated antitumor activity in a mouse cancer model[88]. Alternatively, the generation of CAR T cells against *E. coli* in combination with the seeding of *E. coli* into the TME was shown to robustly control tumors[89]. Mechanistically, the infiltration of a large number of *Lm*-specific CD8 T cells that cannot directly target and kill tumor cells still could control tumors by inducing local tissue damage or impacting the blood vasculature that supports tumor growth[90–92,12,19,77]. Inflammation may also reprogram other immune cells in tumors to become more tumoricidal, which was observed in mouse lung tumor models where influenza infection of the lung conferred reprogramming of alveolar macrophages to protect against tumor development[93]. If such generalized strategies can be effective, it obviates the need to engineer microbes to overexpress patient-specific neoantigens. This will not only save time and reduce costs, but also improve the safety of the therapy by using a reliably tested and generalized biologic. Great potential also exists to improve the effect of the local infection with specially engineered bacteria to boost the inflammatory response against *Lm* to more effectively spread against tumor-specific antigens, as well as combine bacterial-based approaches with other immunomodulatory therapies.

In conclusion, we have shown bacterial immunotherapy can have unintended negative outcomes by driving the accumulation of immunosuppressive cell types within

tumors. However, the tumor promoting impact of *Lm* can be overcome by using a *Lm* dosing regimen that first generates anti-*Lm* CD8 T cells before direct intratumoral administration. The CD8 T cell response against *Lm* can not only remove the immunosuppressive cells from tumors, but also through direct cell killing of non-tumor cells in the TME, promote tumor control. Because the T cell responses against certain pathogens (i.e. *Listeria*, influenza, etc.) have been heavily studied and characterized, these findings have far-reaching consequences and may reveal new applications for existing therapeutics and vaccines. In addition, we show that methods to expand pathogen-specific T cells *ex vivo* for adoptive transfer of bacteria or viral antigen-specific T cells are effective and may be safer than attempting to generate memory T cells by active vaccination in potentially immunocompromised individuals, including cancer patients[94]. Collectively, our study demonstrates new insights into the inefficiencies of current bacterial immunotherapy approaches and reveals a tumor antigen-free, bacterial-based dosing regimen that can control cancer independently of its immunogenicity or the identification of neoantigens.

Acknowledgments:
We thank Russell Vance, Gregory Barton, David Raulet, and Thomas Dubensky for reviewing the manuscript and providing feedback; Hector Nolla, Alma Valleros, Kartoosh Heydari and Anita Wong Lin of the UC Berkeley Cancer Research Laboratory Flow Cytometry Facility. This research was supported by 1DP2CA247830-01 from the National Institutes of Health (NCI) and C23CR5612 from the UC CRCC Cancer Research Coordinating Committee. M.D. is a Pew-Stewart Scholar and a St. Baldrick's Scholar with generous support from Hope with Hazel. J.G.C is a HHMI Gilliam Fellow.

Author Contributions:
Conceptualization and Methodology, M.D., D.A.P., J.G.C., S.F.; Investigation, J.G.C., S.F., T.F.C., J.W., D.G.V., J.Y., N.F.H., E.W., and M.D.; Writing – Original Draft, M.D., J.G.C., S.F.; Writing – Review & Editing, M.D., D.A.P., J.G.C., S.F.; Supervision, M.D., D.A.P., J.G.C., S.F.; Funding Acquisition, M.D., D.A.P.

Declaration of Interests:
D.A.P. is on the board of directors for Laguna Therapeutics.

STAR Methods:
Resource Availability
Lead Contact

Further information and requests for resources and reagents should be directed to and will be fulfilled by the lead contact, Michel DuPage (dupage@berkeley.edu).

Materials availability

Listeria monocytogenes strains used in the study will be made available from the lead contact upon request.

Data and code availability

Any additional information required to reanalyze the data reported in this paper is available from the lead contact upon request.

Experimental models and subject details:

Animal studies

C57BL/6J wildtype mice were obtained from Jackson laboratories (JAX:000664) and bred in house. OT-1 transgenic mice were obtained Taconic (Catalog#: 2334) and bred in house. Prf1$^{-/-}$ mice were a gift from the Stanley lab at the University of California, Berkeley (JAX:000274). Rag2$^{-/-}$ (JAX:008449) and β*2m2m*$^{-/-}$ (JAX:002087) mice were a gift from the Raulet lab at the University of California, Berkeley. Sarcoma cell lines were generated in *Kras*$^{LSL\text{-}G12D/+}$*;p53*$^{fl/fl}$ *mice* by intramuscular injection of the left hind limb with replication-incompetent lentiviruses expressing Cre recombinase as reported previously, harvested, and cultured[71]. For tumor studies, syngeneic C57BL/6J mice were inoculated with 5.0x10^5 MC38 or 2.0x10^5 B16F10 cells in PBS subcutaneously. KP sarcoma cells were inoculated into C57BL/6J mice with 5.0x10^5 cells by intramuscular injection of the right hind limb. Tumor measurements were performed blindly across the entire experiment by a single operator measuring three dimensions of the tumor with calipers three times per week. All the experiments were conducted according to the Institutional Animal Care and Use Committee guidelines of the University of California, Berkeley.

Cell lines

MC38 and B16F10 cell lines were kindly provided by Dr. Jeff Bluestone's lab[95]. MC38-β2m$^{-/-}$ cell line was kindly provided by Dr. David Raulet's lab[40]. All cell lines were maintained in DMEM (GIBCO) supplemented with 10% FBS, sodium pyruvate (GIBCO), 10mM HEPES (GIBCO), and penicillin-streptomycin (GIBCO). Tumor cells were grown at 37□ with 5% CO_2.

Method Details:

Listeria monocytogenes strains

All strains of *L. monocytogenes* were derived from the wild-type 10403S strain. The *Lm* constructs were based on an attenuating deletion of the actA gene (*ΔactA*). *Lm-OVA* expresses an LLO-OVA fusion encompassing amino acids 1-441 of Listeriolysin O

(LLO) and OVA cloned in frame of LLO1-441 under the control of the LLO promoter in the pPL2 integration vector[96]. *Lm-TagRFP* expresses a secreted TagRFP protein under the control of the *actA* promoter using the pPL2 integration vector[46]. All strains were cultured in filter-sterilized nutrient-rich Brain Heart Infusion (BHI) media (BD Biosciences) containing 200 µg/mL streptomycin (Sigma-Aldrich).

Intravenous and Intratumoral *Listeria* infection

Overnight cultures were grown in BHI + 200 µg/mL streptomycin at 30□. The following day, bacteria were grown to logarithmic phase by diluting the overnight culture in fresh BHI + 200 µg/mL streptomycin and culturing at 37□ shaking. Log-phase bacteria were washed and frozen in 9% glycerol/PBS. For intravenous infections, frozen stocks were diluted in PBS to infect via the tail vein with 1 x 10^6 CFU log-phase bacteria. For intravenous infections, frozen stocks were diluted in PBS to infect via intratumoral infections at 5 x 10^7 CFU log-phase bacteria. The mice were euthanized 8-20 days after intratumoral injections and organs were collected for flow analysis.

Colony forming unit assays from tissues

Tissues were collected in 0.1% NP40 buffer diluted in PBS. Organs were homogenized and serially diluted on non-TC treated 96-well plates (Genesee). Serial dilutions were plated on BHI + 200 µg/mL streptomycin plates. Plates were incubated overnight at 37□.

CIN/Primary bone-marrow derived PMN Maintenance and Differentiation:

Cas9+ ER-Hoxb8 conditionally immortalized neutrophils (CINs) were a gift from the Stanley lab at the University of California, Berkeley[60]. CINs were expanded as progenitors in Optimem with 10% FBS, 1% L-glutamine, 30µM 2-mercaptoethanol, and 1% Stem-cell factor (SCF)-producing CHO cell supernatant (CIN Media) that also contained 1µM beta-estradiol in non-TC treated flasks (Genesee) maintaining a concentration less than 1x10^6 cells/mL. Upon reaching the desired quantity, non-adherent progenitors were harvested, washed twice in cold PBS 1x, and plated in non-TC treated flasks containing CIN media lacking beta-estradiol. To generate PMNs, CINs were differentiated until Day 6 in CIN Media + 5ng/mL GM-CSF. To generate PMN-MDSCs, CINs were differentiated in CIN media + 5ng/mL GM-CSF, 40ng/mL IL-6, and 40ng/mL GM-CSF. For primary bone marrow PMNs and PMN-MDSCs, cells were isolated and cultured as described[59]. To generate PMNs-MDSCs, cells were cultured in 40ng/mL IL-6 and 40ng/mL GM-CSF1 day post isolation for 6 days.

In vitro infections:

Cells were infected with *Lm-TagRFP* at an MOI that resulted in 30% of the cells being infected. At 1hr post infection, 50µg/mL Gentamicin was added to kill all extracellular

Listeria. For flow analysis, cells were collected at time points indicated, stained, and fixed with 4% PFA.

Cancer Supernatant Assays

Cancer cell supernatant was generated via the expansion of MC38, B16F10, and 3T3 cell lines in TC-treated flasks in Optimem + 10% FBS, followed by collection of supernatant fluid when cells reached near ~100% confluency. After filtration, all supernatants were frozen down at -20°C. Surveying cancer supernatants involved a 24h incubation period where cells were either re-seeded into TC-treated 24 well plates or non-TC treated flasks in fresh CIN media with a 50:50 ratio of MC38, B16F10, or 3T3 supernatant. Cells were collected at 24h, stained, fixed with 4% PFA, and analyzed by flow cytometry.

Tissue Collection and preparation for Flow cytometry

Flow cytometry was performed on an BD LSR Fortessa X20 (BD Biosciences), CyTEK Aurora (CyTEK Biosciences) or LSRFortessa (BD Biosciences) and datasets were analyzed using FlowJo software (Tree Star). Single cell suspensions were prepared in ice-cold FACS buffer (PBS with 2mM EDTA and 1% BS) and subjected to red blood cell lysis using ACK buffer (150mM NH4Cl, 10mM KHCO3, 0.1mM Na2EDTA, pH7.3). Dead cells were stained with Live/Dead Fixable Blue or Aqua Dead Cell Stain kit (Molecular Probes) in PBS at 4□. Cell surface antigens were stained at 4□ using a mixture of fluorophore-conjugated antibodies. Surface marker stains for murine samples were carried out with anti-mouse CD3 (17A2, BioLegend), anti-mouse CD4 (RM4-5, BioLegend), anti-mouse CD8a (53-6.7, BioLegend), anti-mouse, CD44 (IM7, BioLeged), anti-mouse CD45 (30-F11, BioLegend), anti-H-2Kb MuLV p15E Tetramer-KSPWFTTL (MBL), anti-H-Kb-A2/SIINFEKEL tetramer (NIH tetramer core), anti-IAb/NEKYAQAYPNVS tetramer (NIH tetramer core) in PBS, 0.5% BSA. Cells were fixed using the eBioscience Foxp3/Transcription Factor staining buffer set (eBioscience), prior to intracellular staining. Intracellular staining was performed using anti-mouse Foxp3 (FJK-16S, eBioscience), anti-mouse TNF-α (MP6-XT22, BioLegend), anti-mouse IFN-γ (XMG1.2, eBioscience), at 4□, according to manufacturer's instructions. For Lm-TagRFP infected tissues, single cell suspensions were prepared as above, stained using a mixture of fluorophore-conjugated antibodies at 4□, and fixed in 4% PFA. Cells analyzed by flow cytometry the following day to prevent signal loss from flourescent protein. Cells were resuspended in PBS and filtered through a 70-µm nylon mesh before data acquisition. Datasets were analyzed using FlowJo software (Tree Star).

Restimulation Assays

Resected tumors were minced to 1 mm^3 fragments and digested in RPMI media supplemented with 4-(2-hydroxyethyl)-1-piperazi-neethanesulfonic acid (HEPES), 20 mg/mL DNase I (Roche), and 125 U/mL collagenase D (Roche) using an orbital shaker at 37□. Cells from lymphoid organs were prepared by mechanical disruption pressing against a 70-µm nylon mesh. All the cell suspensions were passed through 40 µm filters before in vitro stimulation. Cytokine staining was performed with 3-5x10^6 cells in Opti-MEM media supplemented with Brefeldin A (eBioscience) or 10 ng/mL phorbol 12-myristate 13-acetate (PMA) (Sigma), and 0.25 µM ionomycin (Sigma). Fixation/permeabilization of cells was conducted for intracellular staining using the eBioscience Foxp3 fixation/permeabilization kit (BioLegend) or Tonbo Foxp3 / Transcription Factor Staining Buffer Kit.

Adoptive transfer experiments

For in vitro T cell culture, spleens and lymph nodes were collected from OT-1 transgenic mice or C57BL/6J wildtype (*WT*) or *Prf1*$^{-/-}$ previously vaccinated with 1.0x10^6 CFU *Lm-OVA* 3-4 weeks prior. OT-1s or OVA-responsive CD8s were were activated with 1µg/mL SIINFEKL peptide in DMEM medium supplemented with 10% FBS, non-essential amino acids, sodium pyruvate, L-glutamine, HEPES, 55 µM β-ME and 200 IU/ml recombinant human IL-2 (TECIMTM, Hoffman-La Roche provided by NCI repository, Frederick National Laboratory for Cancer Research). T cells were transferred into WT or Rag2$^{-/-}$ or *B2m*$^{-/-}$ mice by intravenous injection two weeks prior to MC38 or KP sarcoma inoculations.

***In vivo* antibody-mediated cell depletion**

For tumor progression studies, CD8 depletion was achieved by intraperitoneal injection of 200 µg per mouse of the anti-CD8 monoclonal antibody clone YST-169 (Leinco Technologies, Catalog # C2442) two days prior to tumor inoculation, followed by additional doses every 6 days thereafter. For CD4 depletion, intraperitoneal injection of 200 µg/mouse of clone GK1.5 (Leinco Technologies, Catalog: C1333) was done two days prior to tumor inoculation, followed by additional doses every 6 days thereafter. PMN depletion was done by intraperitoneal injection of 200 µg per mouse of the anti-Ly6G monoclonal antibody clone IA8 (Leinco Technologies, Catalog: L280) twice prior to tumor inoculation, followed by additional doses every 2 days.

Statistical Methods

p values were obtained from unpaired two-tailed Student's t tests for all statistical comparisons between two groups, and data were displayed as mean ± SEMs. For multiple comparisons, one-way ANOVA was used. For tumor growth curves, two-way ANOVA was used with Sidak's multiple comparisons test performed at each time point

or by multiple regression analysis p values are denoted in figures by *p < 0.05, **p < 0.01, ***p < 0.001, and ****p < 0.0001.

Figure Legends:

Figure 1 | Intratumoral injection of *Lm* leads to increased tumor growth and persistent colonization of *Lm* within tumors.

(A) Experimental design.

(B-C) C57BL/6J WT mice were injected with $5x10^5$ MC38 (B, data shown from n= 4-5 mice per group from one of three experiments) or $2x10^5$ B16F10 (C, data shown from n=4-5 mice per group from one of two experiments) tumor cells and then $5x10^7$ *Lm* CFUs IT 11 days later and tumors measured.

(D-E) CFU analysis for *Lm* from indicated tissues after injection IT (D, $5x10^7$ CFU, n=4-8 mice pooled from two experiments) or IV (E, $1x10^6$ CFU, n=4-5 mice pooled from two experiments) of *Lm* 11 days after MC38 or B16F10 tumor inoculation. tdLN = tumor-draining lymph node, ndLN = non-tumor-draining LN.

For all plots, *P<0.05, **P<0.01 by two-way ANOVA, mean ± s.e.m.

Figure 2 | *Lm* localizes in intratumoral PMNs.

(A) Schematic of Tag-RFP expression from *Lm-RFP*.

(B) Representative flow plots of single cell suspensions from MC38 tumors 4 hours post IT of *Lm* (left) or *Lm-RFP* (right) showing CD45 staining versus Tag-RFP fluorescence.

(C) Proportion of RFP^+ cells (C) from MC38 tumors 4 hours (left) or 24 hours (right) after IT *Lm* (representative data from three experiments with n= 3-6 mice/group).

(D) Flow analysis of Tag-RFP localization in PMNs and TAMs at 1, 3, and 5 days after IT *Lm* in MC38 tumors (representative data from two experiments with n= 3-6 mice/group).

(E) Frequency of $Ly6G^+$ PMNs in spleen and MC38 tumors 4 and 24 hours after IT *Lm* or IT PBS.

(F-G) Frequency of intratumoral $Ly6G^+$ PMNs that were RFP^+ (F) or $CD14^+$ (G) at 4 and 24 hours after IT *Lm*.

(H) Frequency of RFP^+Ly6G^+ PMNs that were $CD14^+$ at 4 and 24 hours after IT *Lm*.

Results for D-H are pooled from three experiments with n= 2-5 mice/group per experiment.

For all plots, mean ± s.e.m. and *P<0.05, **P<0.01, ***P<0.001 by two-way ANOVA (D-E) or student t-test (F, G, H).

Figure 3 | PMN conversion into MDSCs permits *Lm* infection and promotes tumor growth.

(A) Experimental strategy and representative flow plots for *in vitro* differentiation of conditionally immortalized neutrophil (CIN) progenitors into PMNs or PMN-MDSCs.
(B) PMNs (left) or PMN-MDSCs (right) derived from CINs were cultured in supernatants from 3T3, MC38, or B16F10 cells for 24 hours *in vitro* and the frequency of $CD14^+$PD-$L1^+$ cells was assessed (representative of two experiments).
(C) Heterogeneous PMN-MDSCs differentiated from CINs as in (A) were infected with *Lm-RFP in vitro* and Tag-RFP^+ cells were identified 2, 4, or 8 hours later in all cells (Total PMNs), $CD14^+$ cells, or $CD14^-$ cells by flow cytometry (representative of three experiments).
(D) Experimental design to deplete PMNs prior to IT PBS or IT *Lm* and measure tumors.
(E) Tumor growth measured in mice injected IT with PBS (left) or IT *Lm* (right) that were treated with isotype control or anti-Ly6G-depleting antibodies prior to tumor inoculation and throughout the experiment (n=5 mice/group).
(F) Representative flow plots of IFNγ production from OT-I CD8 T cells.
(G) Percent of $IFN\gamma^+$ OT-1 CD8 T cells after 24 hours of co-culture with MC38 or MC38-OVA tumor cells in the presence or absence of FACS-purified PMN-MDSCs from IT *Lm* MC38 tumors. Cells were plated at a 1:1 ratio of OT-1 T cells to PMN-MDSCs.
For all plots, *P<0.05, **P<0.01, ***P<0.001 by one-way Anova (B, F) or two-way ANOVA (C, E), mean ± s.e.m for *in vivo* experiments (E) or mean ± s.d. for *in vitro* experiments (B-C, G).

Figure 4 | IV+IT *Lm* controls multiple tumor types while clearing intratumoral bacteria and PMN-MDSCs from tumors.
(A) Experimental strategy for IV+IT *Lm* dosing regimen.
(B-C) IV+IT PBS versus IV+IT *Lm* regimen and growth of MC38 (B, data shown from n= 4-5 mice per group from one of three experiments) and B16F10 (C, data shown from n= 5-6 mice per group from one of two experiments) tumors.
(D) Frequency of $Ly6G^+$ PMNs of all $CD45^+$ cells one day (left) and 5 days (right) after *Lm* IT in IV+IT *Lm* regimen (data shown from n= 5 mice per group from two pooled experiments).
(E) Percent of $Ly6G^+$ PMNs that were $CD14^+$ 1 day (left) and 5 days (right) after IT *Lm* in IV+IT *Lm* regimen.
(F) CFU analysis for *Lm* after IV+IT *Lm* regimen in MC38 tumor-bearing mice. Organs were harvested 4 hours, 12 hours, and on days 1, 3, 5, 10, 15, and 20 after IT *Lm* administration.
(G) Experimental design for comparing prophylactic IV Lm (memory IV+IT) to standard IV+IT *Lm* dosing regimen.
(H) MC38 tumor growth in the setting of memory IV+IT, memory IV only, and memory IV+SubQ *Lm* (injected on opposing flank) compared to PBS treatment or standard IV+IT *Lm*.

(I) Orthotopic KP sarcoma growth with PBS versus a memory IV+IT *Lm* dosing regimen. For all plots, *P<0.05, **P<0.01, ***P<0.001 by student t-test (C, D, E) or two-way ANOVA (B, C, H, I), mean ± s.e.m.

Figure 5 | $CD8^+$ T cells are required for tumor control with IV+IT *Lm*.

(A) Experimental strategy for IV+IT *Lm* dosing regimen followed by early or late flow cytometry analysis.

(B-C) Frequency of intratumoral $CD8^+$ (B) or $CD4^+$ (C) T cells of $CD45^+$ cells from MC38 tumors at early (left) or late (right) timepoints as specified in (A) (results pooled from four experiments with 5 mice/group).

(D) Representative flow plots for IFNγ and TNFα intracellular cytokine staining from intratumoral CD8 T cells 8 days after IT *Lm* or IT PBS administration in each *Lm* dosing regimen (results pooled from two experiments with 5 mice/group).

(E) Experimental strategy for IV+IT *Lm* dosing regimen plus anti-CD8, anti-CD4, or both depleting antibodies beginning 10 days after MC38 tumor inoculation.

(F) MC38 tumor growth with T cell depletion.

(G) Frequency of intratumoral $Ly6G^+$ PMNs of $CD45^+$ cells in IV+IT *Lm* treated mice +/- anti-CD8 depleting antibodies at end of experiment from (F).

(H) MC38 tumor growth in WT versus *Batf3*$^{-/-}$ mice treated with IV+IT *Lm*.

For all plots, *P<0.05, **P<0.01, ***P<0.001 by student t-test (B-C, G), one-way ANOVA (D), or two-way ANOVA (F, H), mean ± s.e.m.

Figure 6 | Anti-*Listeria* CD8 immunity mediates tumor control.

(A) Experimental design to analyze tumor-specific versus *Lm*-specific CD8 T cells after IV+IT *Lm*. OVA was expressed from *Lm* as a surrogate *Lm* antigen.

(B-C) Frequency (left) and total number (right) of tumor-specific (B, MuLV-$H2K^b$ tetramer) and *Lm*-specific (C, SIIN-$H2K^b$ tetramer) CD8 T cells from MC38 tumors 8 days after IT *Lm-OVA* in IV+IT *Lm-OVA* regimen.

(D) MC38-$B2m^{-/-}$ tumor growth after IV+IT *Lm* or IV+IT PBS.

(E) Experimental strategy to adoptively transfer *in vitro*-activated OT-I CD8 T cells in place of prophylactic IV *Lm.*

(F-I) OT-I CD8 T cells were adoptively transferred and MC38 tumors measured after IT PBS, *Lm*, or *Lm-OVA*.

(F) IT PBS, *Lm*, or *Lm-OVA* were compared against standard IV+IT without OT-I transfer (n= 5-6 mice/group from one of two experiments).

(G) As in (F) but using an orthotopic KP sarcoma model (n= 5-6 mice/group).

(H) As in (F) but in *Rag2*$^{-/-}$ mice (n= 5-6 mice/group).

(I) As in (F) but IT delivery compared MC38 tumors grown in WT or $\beta2m^{-/-}$ mice (left) or MC38-*B2m*$^{-/-}$ tumors grown in WT or $\beta2m^{-/-}$ mice (right) (n= 5-6 mice per group).

(J) Experimental strategy to adoptively transfer *in vitro* expanded SIIN-specific CD8 T cells from WT or *Prf1*$^{-/-}$ mice immunized with *Lm-OVA* (see methods).
(K) MC38 tumor growth after adoptive transfer of SIIN-specific CD8 T cells from WT or *Prf1*$^{-/-}$ mice followed by IT injection of PBS, *Lm*, or *Lm-OVA* at day 11 of tumor growth (n= 6 mice/group from one of two experiments).
For all plots, *P<0.05, **P<0.01, ***P<0.001 by student t-test (B, C) or or two-way ANOVA (D, F-H, I, K), mean ± s.e.m.

Figure S1 | Intravenous injection of *Lm* alone does not slow tumor growth.
(A) Experimental design.
(B-C) C57BL/6J WT mice were injected with $5x10^5$ MC38 (B, data shown from n= 5 mice per group from one of three experiments) or $2x10^5$ B16F10 (C, data shown from n= 5 mice per group from one of two experiments) tumor cells and then $1x10^6$ *Lm* CFUs IV 4 days later and tumors measured.
(D) CFU analysis for *Lm* in MC38 tumors from mice injected IV with $1x10^6$ CFU 4 days after tumor inoculation showed seeding and persistence of *Lm* in tumors as in (B) (n=4-5 mice per time point).
For all plots, statistical analysis was done by two-way ANOVA, mean ± s.e.m.

Figure S2 | Population analysis during intratumoral *Lm* infection in MC38 and B16F10 tumors.
(A) Gating strategy for identifying immune cell subsets from single cell suspension of MC38 tumor.
(B) Proportion of immune cell types that were $CD45^+RFP^+$ from B16F10 tumors 24 hours after IT *Lm* (n= 4-5 mice/ group).
(C-D) Frequency of intratumoral immune cell populations as percent of all $CD45^+$ cells 24 hours after IT *Lm* injection in MC38 (C) or B16F10 (D) tumors (n=4-5 mice/group).
(E) Frequency of $Ly6G^+$ PMNs in spleen and B16F10 tumors 24 hours after IT PBS or IT *Lm* (n=4-5 mice/group).
(F-G) Frequency of intratumoral $Ly6G^+$ PMNs that were RFP^+ (F) or $CD14^+$ (G) at 24 hours after IT *Lm* in B16F10 tumors.
(H) Frequency of RFP^+Ly6G^+ PMNs that were $CD14^+$ 24 hours after IT *Lm* into B16F10 tumors.
For all plots, mean ± s.e.m. and *P<0.05, **P<0.01, ***P<0.001 by student t-test (B, C, E, F, G, H).

Figure S3 | PMN-MDSCs are permissive to *Lm* infection.
(A) Representative flow cytometry plots of the differentiation of primary bone marrow progenitors into $CD14^+$ PMN-MDSCs *in vitro* by culturing with IL-6 and GM-CSF.

(B) Heterogeneous PMN-MDSCs differentiated from bone marrow progenitors as in (A) were infected with *Lm-RFP in vitro* and Tag-RFP$^+$ cells were identified 4 or 8 hours later in all cells (Total PMNs), CD14$^+$ cells, or CD14$^-$ cells by flow cytometry.
(C) Frequency of intratumoral immune cell populations as percent of all CD45$^+$ cells 24 hours after IT *Lm* or IT PBS into MC38 tumors in mice pre-treated with isotype or anti-Ly6G (PMN-depleting) antibodies as shown in Figure 3D.
(D) *Lm* CFUs recovered from tumors 20 days after IT *Lm* in mice treated with isotype control or anti-Ly6G antibodies as shown in Figure 3D.
(E) Proportion of immune cell types that were RFP$^+$ from MC38 tumors treated with an isotype control (left) or anti-Ly6G antibody (right) 24 hours after IT *Lm*.
For all plots, *P<0.05, **P<0.01, ***P<0.001 by student t-test, mean ± s.e.m for *in vivo* experiments (C, D) or one-way ANOVA, mean ± s.d for *in vitro* experiments (B).

Figure S4 | IV+IT *Lm* is not impacted by PMN depletion and IV+IT regimen leads to *Lm* clearance.
(A) MC38 tumor growth with PBS versus IV+IT *Lm* and with or without anti-Ly6G depleting antibody treatment beginning two days prior to IT *Lm* administration (n=4-6 mice per group).
(B) CFU analysis for *Lm* in KP sarcomas from experiment depicted in Figure 4I.
For all plots, **P<0.05, **P<0.01, ***P<0.001 by two-way ANOVA (A-C), mean ± s.e.m.

Figure S5 | IV+IT *Lm* dosing regimen reduce intratumoral Treg frequencies but does not impact T cell frequencies in the spleen.
(A-B) Frequency of CD8$^+$ (C) and CD4$^+$ (D) T cells from spleens at early or late timepoints.
(C) Frequency of intratumoral Foxp3$^+$ Tregs of CD4$^+$ cells from MC38 tumors at early (left) or late (right) timepoints as specified in Figure 5A.
(D) Frequency of Foxp3$^+$ Tregs of CD4$^+$ cells from spleens at early (left) or late (right) timepoints.
All data pooled from XX experiments with n=XX mice/group. For all plots timepoints are the same as what was described in Figure 5A. For all plots, *P<0.05, **P<0.01, ***P<0.001 by student t-test (A-D), mean ± s.e.m.

Figure S6 | *Lm*-specific CD8 T cells are present in tumors independent of Prf1 genotype.
(A) Representative flow plots for SIIN-H2K^b tetramer staining from tumors of mice treated with IV+IT PBS compared to IV+IT *Lm-OVA* 8 days after IT injections.
(B) Representative flow plots for MuLV-H2K^b tetramer staining in lymph nodes from naive mice compared to MC38 tumor-bearing mice 19 days post tumor inoculation.

(C) Frequency of intratumoral OT-I CD8 T cells in mice 20 days after IT *Lm* administration from Figure 6I.
(D) CFU analysis for *Lm* in tumors from Figure 6I.
(E) Frequency of intratumoral SIIN-specific CD8 T cells in mice 20 days after IT *Lm* administration from experiments depicted in Figures 6J-K (pooled from two independent experiments).
For all plots, *P<0.05, **P<0.01, ***P<0.001 by student t-test (C,D) or one-way ANOVA (E), mean ± s.e.m.

References

1. McCarthy, E. F. The Toxins of William B. Coley and the Treatment of Bone and Soft-Tissue Sarcomas. *Iowa Orthop. J.* **26**, 154 (2006).
2. Hc, N., Ga, F. & Fh, B. A review of the influence of bacterial infection and of bacterial products (Coley's toxins) on malignant tumors in man; a critical analysis of 30 inoperable cases treated by Coley's mixed toxins, in which diagnosis was confirmed by microscopic examination selected for special study. *Acta Med. Scand. Suppl.* **276**, (1953).
3. Hoption Cann, S. A., van Netten, J. P. & van Netten, C. Dr William Coley and tumour regression: a place in history or in the future. *Postgrad. Med. J.* **79**, 672 (2003).
4. Jiang, S. & Redelman-Sidi, G. BCG in Bladder Cancer Immunotherapy. *Cancers* **14**, 3073 (2022).
5. Yu, Y. A. *et al.* Visualization of tumors and metastases in live animals with bacteria and vaccinia virus encoding light-emitting proteins. *Nat. Biotechnol.* **22**, 313–320 (2004).
6. Kang, S.-R. *et al.* Imaging of tumor colonization by Escherichia coli using 18F-FDS PET. *Theranostics* **10**, 4958 (2020).
7. Fu, A. *et al.* Tumor-resident intracellular microbiota promotes metastatic colonization in breast cancer. *Cell* **185**, (2022).
8. Riquelme, E. *et al.* Tumor Microbiome Diversity and Composition Influence Pancreatic Cancer Outcomes. *Cell* **178**, (2019).
9. Poore, G. D. *et al.* Microbiome analyses of blood and tissues suggest cancer diagnostic approach. *Nature* **579**, (2020).
10. Pushalkar, S. *et al.* The Pancreatic Cancer Microbiome Promotes Oncogenesis by Induction of Innate and Adaptive Immune Suppression. *Cancer Discov.* **8**, (2018).
11. Jin, C. *et al.* Commensal Microbiota Promote Lung Cancer Development via γδ T Cells. *Cell* **176**, (2019).
12. Pawelek, J. M., Low, K. B. & Bermudes, D. Tumor-targeted Salmonella as a novel anticancer vector. *Cancer Res.* **57**, (1997).
13. Dang, L. H., Bettegowda, C., Huso, D. L., Kinzler, K. W. & Vogelstein, B.

Combination bacteriolytic therapy for the treatment of experimental tumors. *Proc. Natl. Acad. Sci. U. S. A.* **98**, (2001).

14. Honda, K. & Littman, D. R. The microbiota in adaptive immune homeostasis and disease. *Nature* **535**, 75–84 (2016).
15. Zhou, M. *et al.* Bacteria-based immunotherapy for cancer: a systematic review of preclinical studies. *Front. Immunol.* **14**, (2023).
16. Riglar, D. T. & Silver, P. A. Engineering bacteria for diagnostic and therapeutic applications. *Nat. Rev. Microbiol.* **16**, 214–225 (2018).
17. Chowdhury, S. *et al.* Programmable bacteria induce durable tumor regression and systemic antitumor immunity. *Nat. Med.* **25**, (2019).
18. Din, M. O. *et al.* Synchronized cycles of bacterial lysis for in vivo delivery. *Nature* **536**, (2016).
19. Deng, W. *et al.* Recombinant *Listeria* promotes tumor rejection by $CD8^+$ T cell-dependent remodeling of the tumor microenvironment. *Proc. Natl. Acad. Sci. U. S. A.* **115**, 8179–8184 (2018).
20. Kim, S. H. *et al.* Mage-b vaccine delivered by recombinant Listeria monocytogenes is highly effective against breast cancer metastases. *Br. J. Cancer* **99**, 741 (2008).
21. Listeria as a vaccine vector. *Microbes Infect.* **9**, 1226–1235 (2007).
22. Ding, Y. D. *et al.* Listeria monocytogenes: a promising vector for tumor immunotherapy. *Front. Immunol.* **14**, (2023).
23. Pan, Z.-K., Ikonomidis, G., Lazenby, A., Pardoll, D. & Paterson, Y. A recombinant Listeria monocytogenes vaccine expressing a model tumour antigen protects mice against lethal tumour cell challenge and causes regression of established tumours. *Nat. Med.* **1**, 471–477 (1995).
24. Nguyen, D. H., Chong, A., Hong, Y. & Min, J. J. Bioengineering of bacteria for cancer immunotherapy. *Nat. Commun.* **14**, (2023).
25. Hassan, R. *et al.* Clinical Response of Live-Attenuated, Listeria monocytogenes Expressing Mesothelin (CRS-207) with Chemotherapy in Patients with Malignant Pleural Mesothelioma. *Clin. Cancer Res.* **25**, 5787–5798 (2019).
26. Le, D. T. *et al.* Safety and survival with GVAX pancreas prime and Listeria Monocytogenes-expressing mesothelin (CRS-207) boost vaccines for metastatic pancreatic cancer. *J. Clin. Oncol.* **33**, (2015).
27. Huh, W. K. *et al.* Phase II study of axalimogene filolisbac (ADXS-HPV) for platinum-refractory cervical carcinoma: An NRG oncology/gynecologic oncology group study. *Gynecol. Oncol.* **158**, (2020).
28. Basu, P. *et al.* A Randomized Phase 2 Study of ADXS11-001 Listeria monocytogenes-Listeriolysin O Immunotherapy With or Without Cisplatin in Treatment of Advanced Cervical Cancer. *Int. J. Gynecol. Cancer* **28**, (2018).
29. Drake, C. G. *et al.* Safety and preliminary immunogenicity of JNJ-64041809, a live-attenuated, double-deleted Listeria monocytogenes-based immunotherapy, in

metastatic castration-resistant prostate cancer. *Prostate Cancer Prostatic Dis.* **25**, (2022).

30. Stein, M. N. *et al.* ADXS31142 Immunotherapy ± Pembrolizumab Treatment for Metastatic Castration-Resistant Prostate Cancer: Open-Label Phase I/II KEYNOTE-046 Study. *Oncologist* **27**, (2022).
31. Moreno Ayala, M. A., Li, Z. & DuPage, M. Treg programming and therapeutic reprogramming in cancer. *Immunology* **157**, 198–209 (2019).
32. Veglia, F., Sanseviero, E. & Gabrilovich, D. I. Myeloid-derived suppressor cells in the era of increasing myeloid cell diversity. *Nat. Rev. Immunol.* **21**, 485–498 (2021).
33. Li, K. *et al.* Myeloid-derived suppressor cells as immunosuppressive regulators and therapeutic targets in cancer. *Signal Transduction and Targeted Therapy* **6**, (2021).
34. Binnewies, M. *et al.* Understanding the tumor immune microenvironment (TIME) for effective therapy. *Nat. Med.* **24**, (2018).
35. Perry, C. J. *et al.* Myeloid-targeted immunotherapies act in synergy to induce inflammation and antitumor immunity. *J. Exp. Med.* **215**, 877–893 (2018).
36. Cao, L. L. & Kagan, J. C. Targeting innate immune pathways for cancer immunotherapy. *Immunity* **56**, (2023).
37. Uher, O. *et al.* Coley's immunotherapy revived: Innate immunity as a link in priming cancer cells for an attack by adaptive immunity. *Semin. Oncol.* **46**, (2019).
38. Marabelle, A., Kohrt, H., Caux, C. & Levy, R. Intratumoral immunization: a new paradigm for cancer therapy. *Clin. Cancer Res.* **20**, (2014).
39. Frank, M. J. *et al.* In Situ Vaccination with a TLR9 Agonist and Local Low-Dose Radiation Induces Systemic Responses in Untreated Indolent Lymphoma. *Cancer Discov.* **8**, (2018).
40. Nicolai, C. J. *et al.* NK cells mediate clearance of CD8+ T cell-resistant tumors in response to STING agonists. *Science immunology* **5**, (2020).
41. Lee, W. S. *et al.* Original research: Intratumoral immunotherapy using a TLR2/3 agonist, L-pampo, induces robust antitumor immune responses and enhances immune checkpoint blockade. *Journal for Immunotherapy of Cancer* **10**, (2022).
42. Xu, G. *et al.* Listeria-based hepatocellular carcinoma vaccine facilitates anti-PD-1 therapy by regulating macrophage polarization. *Oncogene* **39**, 1429–1444 (2019).
43. Wang, Y. *et al.* Adjuvant effect of the novel TLR1/TLR2 agonist Diprovocim synergizes with anti-PD-L1 to eliminate melanoma in mice. *Proc. Natl. Acad. Sci. U. S. A.* **115**, E8698–E8706 (2018).
44. Corrales, L. *et al.* Direct Activation of STING in the Tumor Microenvironment Leads to Potent and Systemic Tumor Regression and Immunity. *Cell Rep.* **11**, (2015).
45. Oladejo, M., Paterson, Y. & Wood, L. M. Clinical Experience and Recent Advances in the Development of Listeria-Based Tumor Immunotherapies. *Front. Immunol.* **12**, 642316 (2021).
46. Brockstedt, D. G. *et al.* Listeria-based cancer vaccines that segregate

immunogenicity from toxicity. *Proc. Natl. Acad. Sci. U. S. A.* **101**, 13832–13837 (2004).

47. Waite, J. C. *et al.* Dynamic imaging of the effector immune response to listeria infection in vivo. *PLoS Pathog.* **7**, (2011).
48. Moors, M. A., Levitt, B., Youngman, P. & Portnoy, D. A. Expression of listeriolysin O and ActA by intracellular and extracellular Listeria monocytogenes. *Infect. Immun.* **67**, (1999).
49. Czuprynski, C. J., Henson, P. M. & Campbell, P. A. Killing of Listeria monocytogenes by Inflammatory Neutrophils and Mononuclear Phagocytes From Immune and Nonimmune Mice. *J. Leukoc. Biol.* **35**, 193–208 (1984).
50. Witter, A. R., Okunnu, B. M. & Berg, R. E. The Essential Role of Neutrophils during Infection with the Intracellular Bacterial Pathogen Listeria monocytogenes. *J. Immunol.* **197**, 1557–1565 (2016).
51. Okunnu, B. M. & Berg, R. E. Neutrophils Are More Effective than Monocytes at Phagosomal Containment and Killing of Listeria monocytogenes. *ImmunoHorizons* **3**, (2019).
52. Shaul, M. E. & Fridlender, Z. G. Neutrophils as active regulators of the immune system in the tumor microenvironment. *J. Leukoc. Biol.* **102**, 343–349 (2017).
53. Powell, D. R. & Huttenlocher, A. Neutrophils in the Tumor Microenvironment. *Trends Immunol.* **37**, 41–52 (2016).
54. Wu, Y., Yi, M., Niu, M., Mei, Q. & Wu, K. Myeloid-derived suppressor cells: an emerging target for anticancer immunotherapy. *Mol. Cancer* **21**, 1–19 (2022).
55. Hegde, S., Leader, A.M., Merad, M. MDSC: Markers, development, states, and unaddressed complexity. *Immunity* **54**, 875–884 (2021).
56. Bronte, V. *et al.* Recommendations for myeloid-derived suppressor cell nomenclature and characterization standards. *Nat. Commun.* **7**, 1–10 (2016).
57. Wang, C. *et al.* CD300ld on neutrophils is required for tumour-driven immune suppression. *Nature* **621**, (2023).
58. Veglia, F. *et al.* Analysis of classical neutrophils and polymorphonuclear myeloid-derived suppressor cells in cancer patients and tumor-bearing mice. *J. Exp. Med.* **218**, (2021).
59. Eckert, I., Ribechini, E. & Lutz, M. B. In Vitro Generation of Murine Myeloid-Derived Suppressor Cells, Analysis of Markers, Developmental Commitment, and Function. *Myeloid-Derived Suppressor Cells* 99–114 (2021).
60. Roberts, A. W. *et al.* Cas9+ conditionally-immortalized macrophages as a tool for bacterial pathogenesis and beyond. *Elife* **8**, (2019).
61. Chávez-Arroyo, A. & Portnoy, D. A. Why is Listeria monocytogenes such a potent inducer of CD8+ T-cells? *Cell. Microbiol.* **22**, e13175 (2020).
62. Genitourinary cancer neoadjuvant therapies: current and future approaches. *Trends Cancer Res.* **9**, 1041–1057 (2023).

63. Kirsch, D. G. *et al.* A spatially and temporally restricted mouse model of soft tissue sarcoma. *Nat. Med.* **13**, (2007).
64. Waldman, A. D., Fritz, J. M. & Lenardo, M. J. A guide to cancer immunotherapy: from T cell basic science to clinical practice. *Nat. Rev. Immunol.* **20**, 651–668 (2020).
65. Giles, J. R., Globig, A. M., Kaech, S. M. & Wherry, E. J. CD8+ T cells in the cancer-immunity cycle. *Immunity* **56**, (2023).
66. Wang, D. *et al.* Targeting EZH2 Reprograms Intratumoral Regulatory T Cells to Enhance Cancer Immunity. *Cell Rep.* **23**, (2018).
67. Moreno Ayala, M. A. *et al.* CXCR3 expression in regulatory T cells drives interactions with type I dendritic cells in tumors to restrict CD8+ T cell antitumor immunity. *Immunity* **56**, 1613–1630.e5 (2023).
68. Hos, B. J. *et al.* Identification of a neo-epitope dominating endogenous CD8 T cell responses to MC-38 colorectal cancer. *Oncoimmunology* **9**, 1673125 (2019).
69. Liu, D. *et al.* IL-10-Dependent Crosstalk between Murine Marginal Zone B Cells, Macrophages, and CD8α+ Dendritic Cells Promotes Listeria monocytogenes Infection. *Immunity* **51**, 64–76.e7 (2019).
70. Edelson, B. T. *et al.* CD8α(+) dendritic cells are an obligate cellular entry point for productive infection by Listeria monocytogenes. *Immunity* **35**, (2011).
71. DuPage, M., Mazumdar, C., Schmidt, L. M., Cheung, A. F. & Jacks, T. Expression of tumour-specific antigens underlies cancer immunoediting. *Nature* **482**, (2012).
72. Leschner, S. *et al.* Tumor invasion of Salmonella enterica serovar Typhimurium is accompanied by strong hemorrhage promoted by TNF-alpha. *PLoS One* **4**, e6692 (2009).
73. Jiang, S.-N. *et al.* Inhibition of tumor growth and metastasis by a combination of Escherichia coli-mediated cytolytic therapy and radiotherapy. *Mol. Ther.* **18**, 635–642 (2010).
74. Agrawal, N. *et al.* Bacteriolytic therapy can generate a potent immune response against experimental tumors. *Proc. Natl. Acad. Sci. U. S. A.* **101**, (2004).
75. St. Jean, A. T., Swofford, C. A., Panteli, J. T., Brentzel, Z. J. & Forbes, N. S. Bacterial Delivery of Staphylococcus aureus α-Hemolysin Causes Regression and Necrosis in Murine Tumors. *Mol. Ther.* **22**, 1266–1274 (2014).
76. Canale, F. P. *et al.* Metabolic modulation of tumours with engineered bacteria for immunotherapy. *Nature* **598**, (2021).
77. Ahmed, S. G. *et al.* Intratumoral injection of schwannoma with attenuated induces antitumor immunity and controls tumor growth. *Proc. Natl. Acad. Sci. U. S. A.* **119**, e2202719119 (2022).
78. Weibel, S., Stritzker, J., Eck, M., Goebel, W. & Szalay, A. A. Colonization of experimental murine breast tumours by Escherichia coli K-12 significantly alters the tumour microenvironment. *Cell. Microbiol.* **10**, (2008).

79. Quispe-Tintaya, W. *et al.* Nontoxic radioactive Listeria(at) is a highly effective therapy against metastatic pancreatic cancer. *Proc. Natl. Acad. Sci. U. S. A.* **110**, 8668–8673 (2013).
80. Jia, L.-J. *et al.* Enhanced therapeutic effect by combination of tumor-targeting salmonella and endostatin in murine melanoma model. *Cancer Biol. Ther.* (2005) doi:10.4161/cbt.4.8.1891.
81. Westphal, K., Leschner, S., Jablonska, J., Loessner, H. & Weiss, S. Containment of tumor-colonizing bacteria by host neutrophils. *Cancer Res.* **68**, (2008).
82. Kim, M. *et al.* Critical Role for the Microbiota in CX3CR1+ Intestinal Mononuclear Phagocyte Regulation of Intestinal T Cell Responses. *Immunity* **49**, (2018).
83. Selvanesan, B. C. *et al.* Listeria delivers tetanus toxoid protein to pancreatic tumors and induces cancer cell death in mice. *Sci. Transl. Med.* **14**, eabc1600 (2022).
84. Delivery of a viral antigen to the class I processing and presentation pathway by Listeria monocytogenes. *J. Exp. Med.* **180**, 2209 (1994).
85. Biot, C. *et al.* Preexisting BCG-specific T cells improve intravesical immunotherapy for bladder cancer. *Sci. Transl. Med.* **4**, (2012).
86. Raskov, H., Orhan, A., Christensen, J. P. & Gögenur, I. Cytotoxic CD8+ T cells in cancer and cancer immunotherapy. *Br. J. Cancer* **124**, 359–367 (2021).
87. Mittra, S., Harding, S. M. & Kaech, S. M. Memory T Cells in the Immunoprevention of Cancer: A Switch from Therapeutic to Prophylactic Approaches. *J. Immunol.* **211**, 907–916 (2023).
88. Newman, J. H. *et al.* Intratumoral injection of the seasonal flu shot converts immunologically cold tumors to hot and serves as an immunotherapy for cancer. *Proc. Natl. Acad. Sci. U. S. A.* **117**, 1119–1128 (2020).
89. Vincent, R. L. *et al.* Probiotic-guided CAR-T cells for solid tumor targeting. *Science* **382**, 211–218 (2023).
90. Liu, F., Zhang, L., Hoffman, R. M. & Zhao, M. Vessel destruction by tumor-targeting Salmonella typhimurium A1-R is enhanced by high tumor vascularity. *Cell Cycle* **9**, (2010).
91. Spiotto, M. T., Rowley, D. A. & Schreiber, H. Bystander elimination of antigen loss variants in established tumors. *Nat. Med.* **10**, (2004).
92. Wood, L. M. *et al.* Targeting tumor vasculature with novel Listeria-based vaccines directed against CD105. *Cancer Immunol. Immunother.* **60**, 931–942 (2011).
93. Wang, T. *et al.* Influenza-trained mucosal-resident alveolar macrophages confer long-term antitumor immunity in the lungs. *Nat. Immunol.* **24**, 423–438 (2023).
94. Liu, Q., Sun, Z. & Chen, L. Memory T cells: strategies for optimizing tumor immunotherapy. *Protein Cell* **11**, 549–564 (2020).
95. Sockolosky, J. T. *et al.* Selective targeting of engineered T cells using orthogonal IL-2 cytokine-receptor complexes. *Science* **359**, 1037–1042 (2018).
96. Bahjat, K. S. *et al.* Cytosolic entry controls CD8+-T-cell potency during bacterial

infection. *Infect. Immun.* **74**, 6387–6397 (2006).

Figure 1.

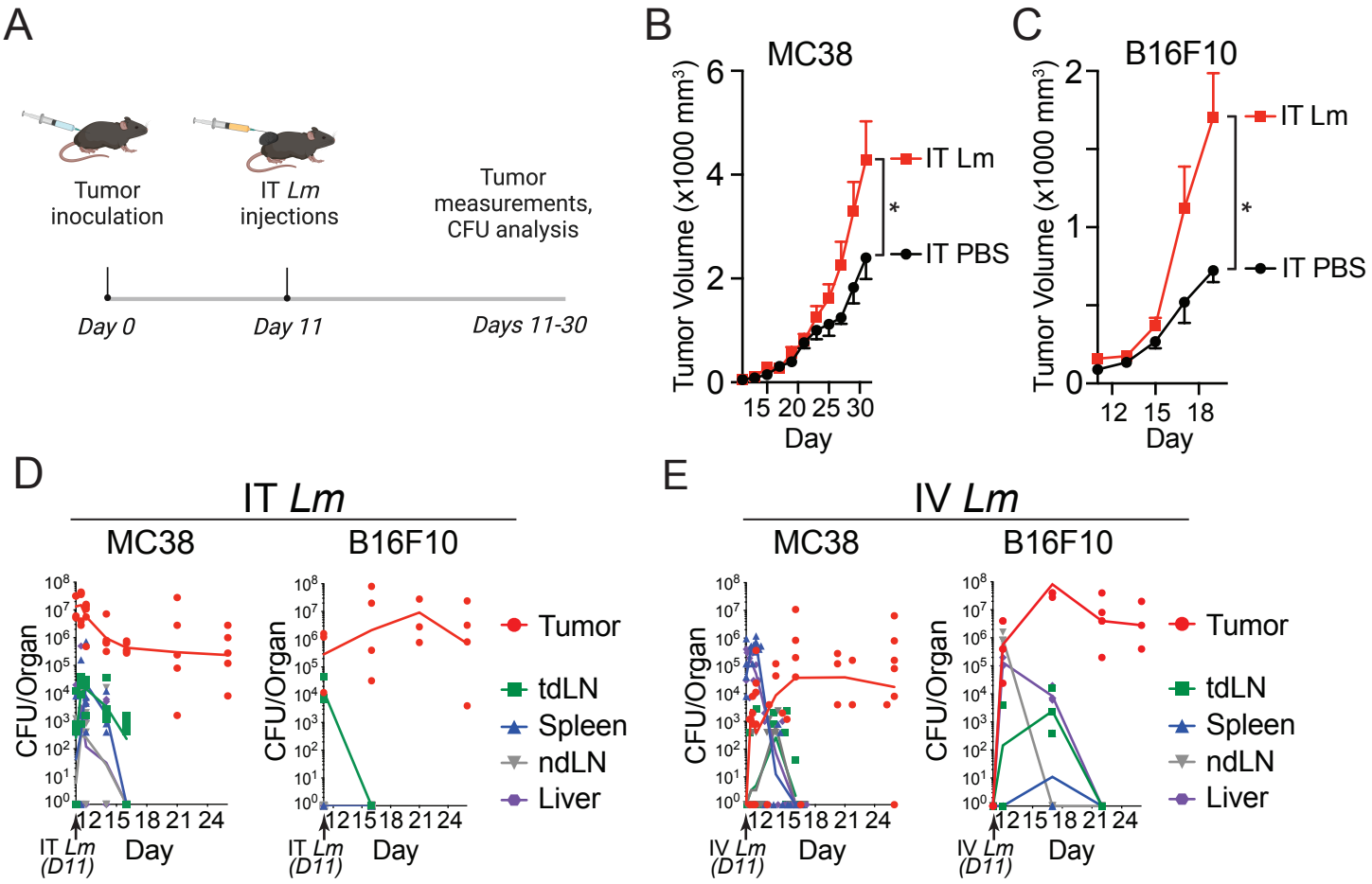
A
Tumor inoculation
IT Lm injections
Tumor measurements, CFU analysis
Day 0
Day 11
Days 11-30
B
MC38
Tumor Volume (x1000 mm³)
Day
IT Lm
IT PBS
*
C
B16F10
Tumor Volume (x1000 mm³)
Day
IT Lm
IT PBS
*
D
IT Lm
MC38
B16F10
CFU/Organ
IT Lm (D11)
Day
Tumor
tdLN
Spleen
ndLN
Liver
E
IV Lm
MC38
B16F10
CFU/Organ
IV Lm (D11)
Day
Tumor
tdLN
Spleen
ndLN
Liver

Figure 1 | Intratumoral injection of *Lm* leads to increased tumor growth and persistent colonization of *Lm* within tumors.

(A) Experimental design.

(B-C) C57BL/6J WT mice were injected with $5x10^5$ MC38 (B, data shown from n= 4-5 mice per group from one of three experiments) or $2x10^5$ B16F10 (C, data shown from n=4-5 mice per group from one of two experiments) tumor cells and then $5x10^7$ *Lm* CFUs IT 11 days later and tumors measured.

(D-E) CFU analysis for *Lm* from indicated tissues after injection IT (D, $5x10^7$ CFU, n=4-8 mice pooled from two experiments) or IV (E, $1x10^6$ CFU, n=4-5 mice pooled from two experiments) of *Lm* 11 days after MC38 or B16F10 tumor inoculation. tdLN = tumor-draining lymph node, ndLN = non-tumor-draining LN.

For all plots, *P<0.05, **P<0.01 by two-way ANOVA, mean ± s.e.m.

Figure 2.

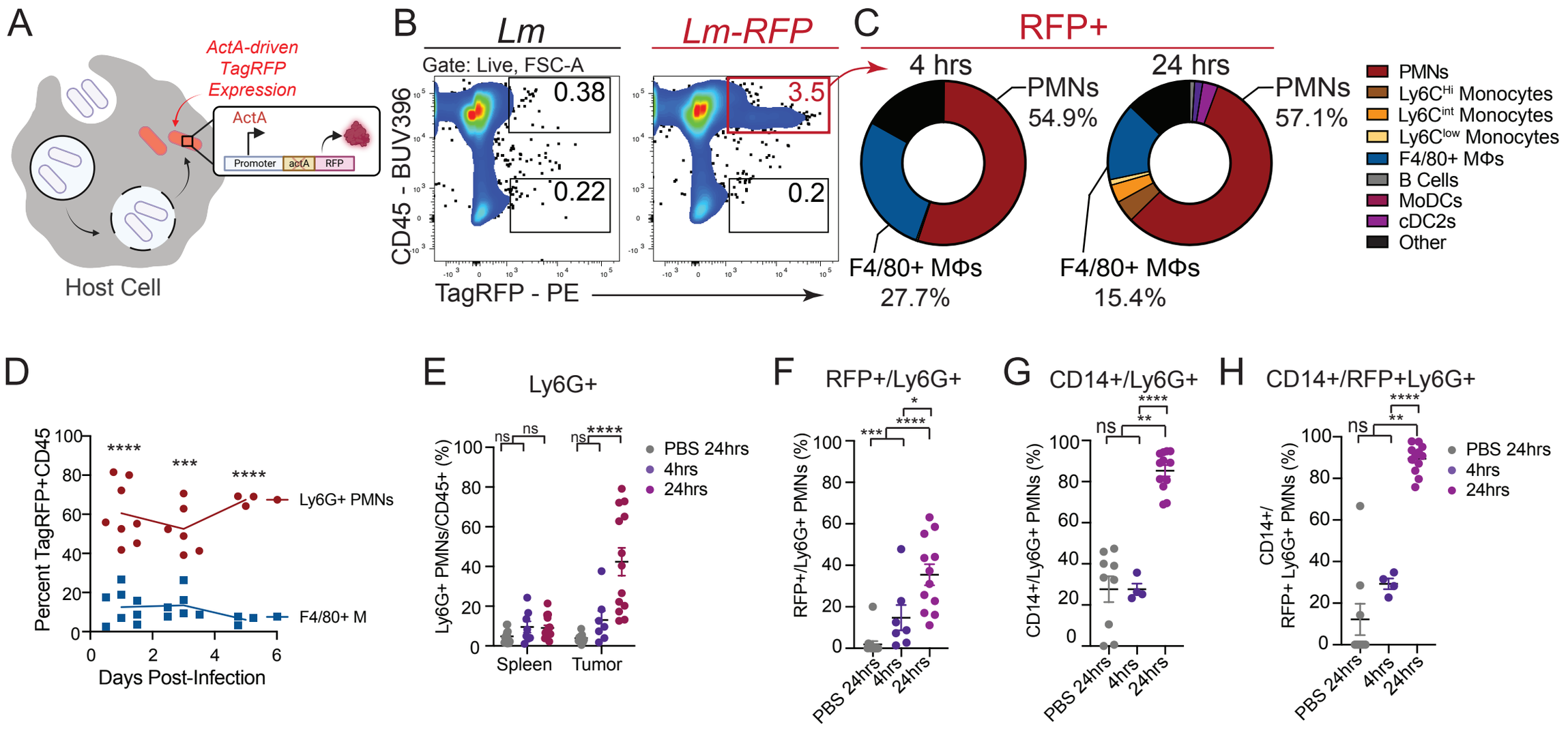
A
ActA-driven TagRFP Expression
ActA
Promoter
actA
RFP
Host Cell
B
Lm
Lm-RFP
Gate: Live, FSC-A
CD45 - BUV396
TagRFP - PE
0.38
0.22
3.5
0.2
C
RFP+
4 hrs
24 hrs
PMNs 54.9%
F4/80+ MΦs 27.7%
PMNs 57.1%
F4/80+ MΦs 15.4%
PMNs
Ly6C^Hi Monocytes
Ly6C^int Monocytes
Ly6C^low Monocytes
F4/80+ MΦs
B Cells
MoDCs
cDC2s
Other
D
Percent TagRFP+CD45
Days Post-Infection
Ly6G+ PMNs
F4/80+ M
E
Ly6G+
Ly6G+ PMNs/CD45+ (%)
Spleen
Tumor
PBS 24hrs
4hrs
24hrs
F
RFP+/Ly6G+
RFP+/Ly6G+ PMNs (%)
G
CD14+/Ly6G+
CD14+/Ly6G+ PMNs (%)
H
CD14+/RFP+Ly6G+
CD14+/ RFP+ Ly6G+ PMNs (%)

Figure 2 | *Lm* localizes in intratumoral PMNs.
(A) Schematic of Tag-RFP expression from *Lm-RFP*.
(B) Representative flow plots of single cell suspensions from MC38 tumors 4 hours post IT of *Lm* (left) or *Lm-RFP* (right) showing CD45 staining versus Tag-RFP fluorescence.
(C) Proportion of RFP^+ cells (C) from MC38 tumors 4 hours (left) or 24 hours (right) after IT *Lm* (representative data from three experiments with n= 3-6 mice/group).
(D) Flow analysis of Tag-RFP localization in PMNs and TAMs at 1, 3, and 5 days after IT *Lm* in MC38 tumors (representative data from two experiments with n= 3-6 mice/group).
(E) Frequency of $Ly6G^+$ PMNs in spleen and MC38 tumors 4 and 24 hours after IT *Lm* or IT PBS.
(F-G) Frequency of intratumoral $Ly6G^+$ PMNs that were RFP^+ (F) or $CD14^+$ (G) at 4 and 24 hours after IT *Lm*.
(H) Frequency of RFP^+Ly6G^+ PMNs that were $CD14^+$ at 4 and 24 hours after IT *Lm*.
Results for D-H are pooled from three experiments with n= 2-5 mice/group per experiment.
For all plots, mean ± s.e.m. and *P<0.05, **P<0.01, ***P<0.001 by two-way ANOVA (D-E) or student t-test (F, G, H).

Figure 3.

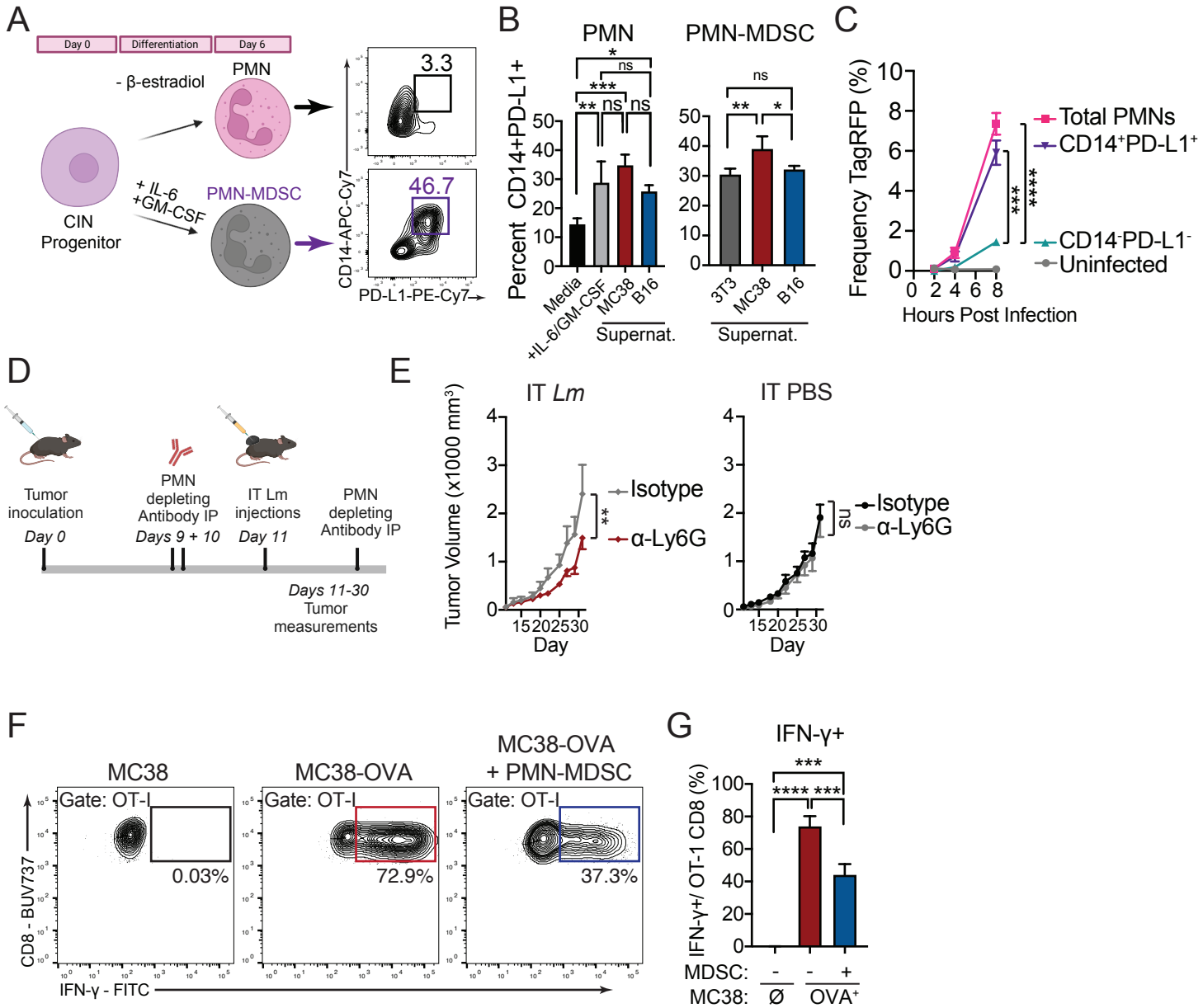
A
Day 0
Differentiation
Day 6
- β-estradiol
PMN
CIN
Progenitor
+ IL-6
+GM-CSF
PMN-MDSC
3.3
46.7
CD14-APC-Cy7
PD-L1-PE-Cy7
B
PMN
PMN-MDSC
Percent CD14+PD-L1+
Media
+IL-6/GM-CSF
MC38
B16
Supernat.
3T3
MC38
B16
Supernat.
C
Frequency TagRFP (%)
Hours Post Infection
Total PMNs
CD14+PD-L1+
CD14-PD-L1-
Uninfected
D
Tumor inoculation
Day 0
PMN depleting Antibody IP
Days 9 + 10
IT Lm injections
Day 11
PMN depleting Antibody IP
Days 11-30
Tumor measurements
E
IT Lm
IT PBS
Tumor Volume (x1000 mm3)
Day
Isotype
α-Ly6G
F
MC38
MC38-OVA
MC38-OVA + PMN-MDSC
Gate: OT-I
0.03%
72.9%
37.3%
CD8 - BUV737
IFN-γ - FITC
G
IFN-γ+
IFN-γ+/ OT-1 CD8 (%)
MDSC:
MC38:
Ø
OVA+

Figure 3 | PMN conversion into MDSCs permits *Lm* infection and promotes tumor growth.

(A) Experimental strategy and representative flow plots for *in vitro* differentiation of conditionally immortalized neutrophil (CIN) progenitors into PMNs or PMN-MDSCs.
(B) PMNs (left) or PMN-MDSCs (right) derived from CINs were cultured in supernatants from 3T3, MC38, or B16F10 cells for 24 hours *in vitro* and the frequency of $CD14^{+}PD\text{-}L1^{+}$ cells was assessed (representative of two experiments).
(C) Heterogeneous PMN-MDSCs differentiated from CINs as in (A) were infected with *Lm-RFP in vitro* and $Tag\text{-}RFP^{+}$ cells were identified 2, 4, or 8 hours later in all cells (Total PMNs), $CD14^{+}$ cells, or $CD14^{-}$ cells by flow cytometry (representative of three experiments).
(D) Experimental design to deplete PMNs prior to IT PBS or IT *Lm* and measure tumors.
(E) Tumor growth measured in mice injected IT with PBS (left) or IT *Lm* (right) that were treated with isotype control or anti-Ly6G-depleting antibodies prior to tumor inoculation and throughout the experiment (n=5 mice/group).
(F) Representative flow plots of IFNγ production from OT-I CD8 T cells.
(G) Percent of $IFN\gamma^{+}$ OT-1 CD8 T cells after 24 hours of co-culture with MC38 or MC38-OVA tumor cells in the presence or absence of FACS-purified PMN-MDSCs from IT *Lm* MC38 tumors. Cells were plated at a 1:1 ratio of OT-1 T cells to PMN-MDSCs.
For all plots, *P<0.05, **P<0.01, ***P<0.001 by one-way Anova (B, F) or two-way ANOVA (C, E), mean ± s.e.m for *in vivo* experiments (E) or mean ± s.d. for *in vitro* experiments (B-C, G).

Figure 4.

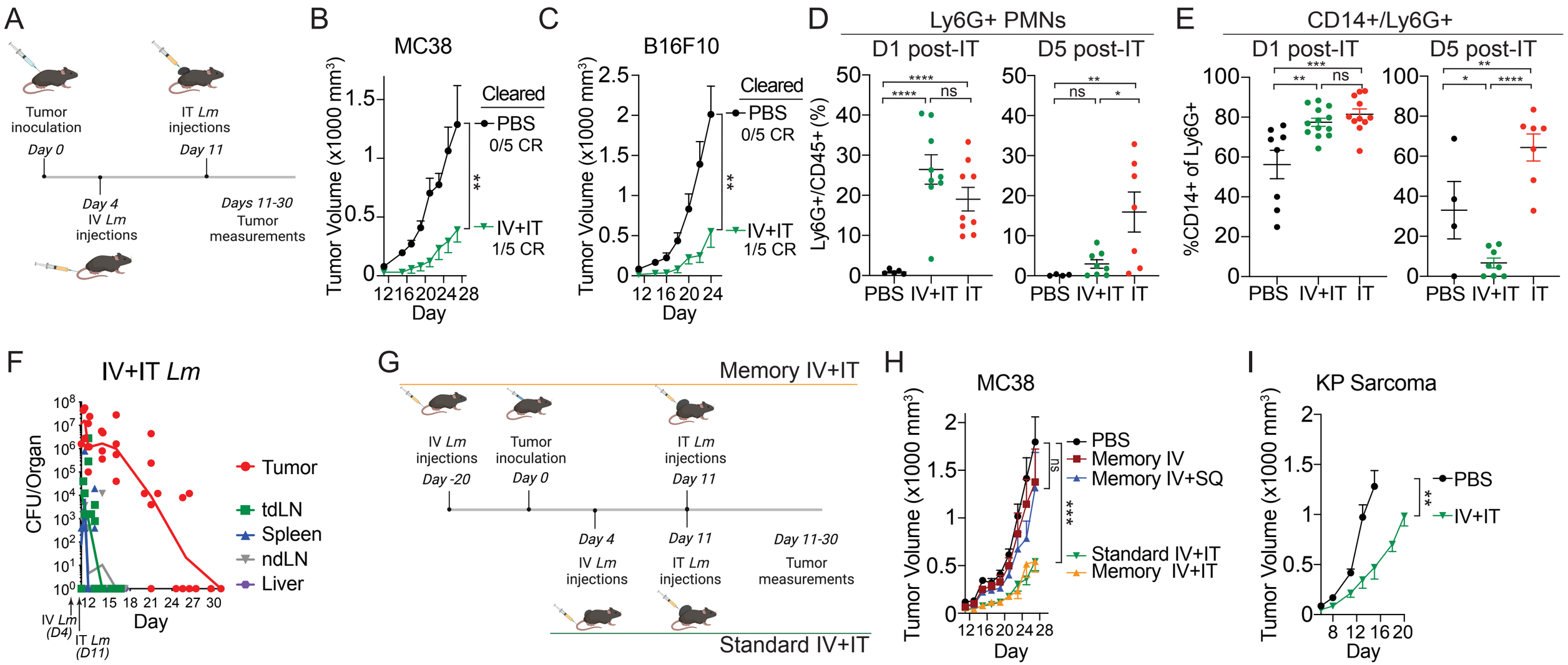
A
Tumor inoculation
Day 0
IT Lm injections
Day 11
Day 4
IV Lm injections
Days 11-30
Tumor measurements
B
MC38
Tumor Volume (x1000 mm³)
Cleared
PBS 0/5 CR
IV+IT 1/5 CR
Day
C
B16F10
Tumor Volume (x1000 mm³)
Cleared
PBS 0/5 CR
IV+IT 1/5 CR
Day
D
Ly6G+ PMNs
D1 post-IT
D5 post-IT
Ly6G+/CD45+ (%)
PBS IV+IT IT
E
CD14+/Ly6G+
D1 post-IT
D5 post-IT
%CD14+ of Ly6G+
PBS IV+IT IT
F
IV+IT Lm
CFU/Organ
Tumor
tdLN
Spleen
ndLN
Liver
Day
IV Lm (D4)
IT Lm (D11)
G
Memory IV+IT
IV Lm injections
Day -20
Tumor inoculation
Day 0
IT Lm injections
Day 11
Day 4
IV Lm injections
Day 11
IT Lm injections
Day 11-30
Tumor measurements
Standard IV+IT
H
MC38
Tumor Volume (x1000 mm³)
PBS
Memory IV
Memory IV+SQ
Standard IV+IT
Memory IV+IT
Day
I
KP Sarcoma
Tumor Volume (x1000 mm³)
PBS
IV+IT
Day

Figure 4 | IV+IT *Lm* controls multiple tumor types while clearing intratumoral bacteria and PMN-MDSCs from tumors.

(A) Experimental strategy for IV+IT *Lm* dosing regimen.

(B-C) IV+IT PBS versus IV+IT *Lm* regimen and growth of MC38 (B, data shown from n= 4-5 mice per group from one of three experiments) and B16F10 (C, data shown from n= 5-6 mice per group from one of two experiments) tumors.

(D) Frequency of $Ly6G^+$ PMNs of all $CD45^+$ cells one day (left) and 5 days (right) after *Lm* IT in IV+IT *Lm* regimen (data shown from n= 5 mice per group from two pooled experiments).

(E) Percent of $Ly6G^+$ PMNs that were $CD14^+$ 1 day (left) and 5 days (right) after IT *Lm* in IV+IT *Lm* regimen.

(F) CFU analysis for *Lm* after IV+IT *Lm* regimen in MC38 tumor-bearing mice. Organs were harvested 4 hours, 12 hours, and on days 1, 3, 5, 10, 15, and 20 after IT *Lm* administration.

(G) Experimental design for comparing prophylactic IV Lm (memory IV+IT) to standard IV+IT *Lm* dosing regimen.

(H) MC38 tumor growth in the setting of memory IV+IT, memory IV only, and memory IV+SubQ *Lm* (injected on opposing flank) compared to PBS treatment or standard IV+IT *Lm*.

(I) Orthotopic KP sarcoma growth with PBS versus a memory IV+IT *Lm* dosing regimen.

For all plots, *P<0.05, **P<0.01, ***P<0.001 by student t-test (C, D, E) or two-way ANOVA (B, C, H, I), mean ± s.e.m.

Figure 5.

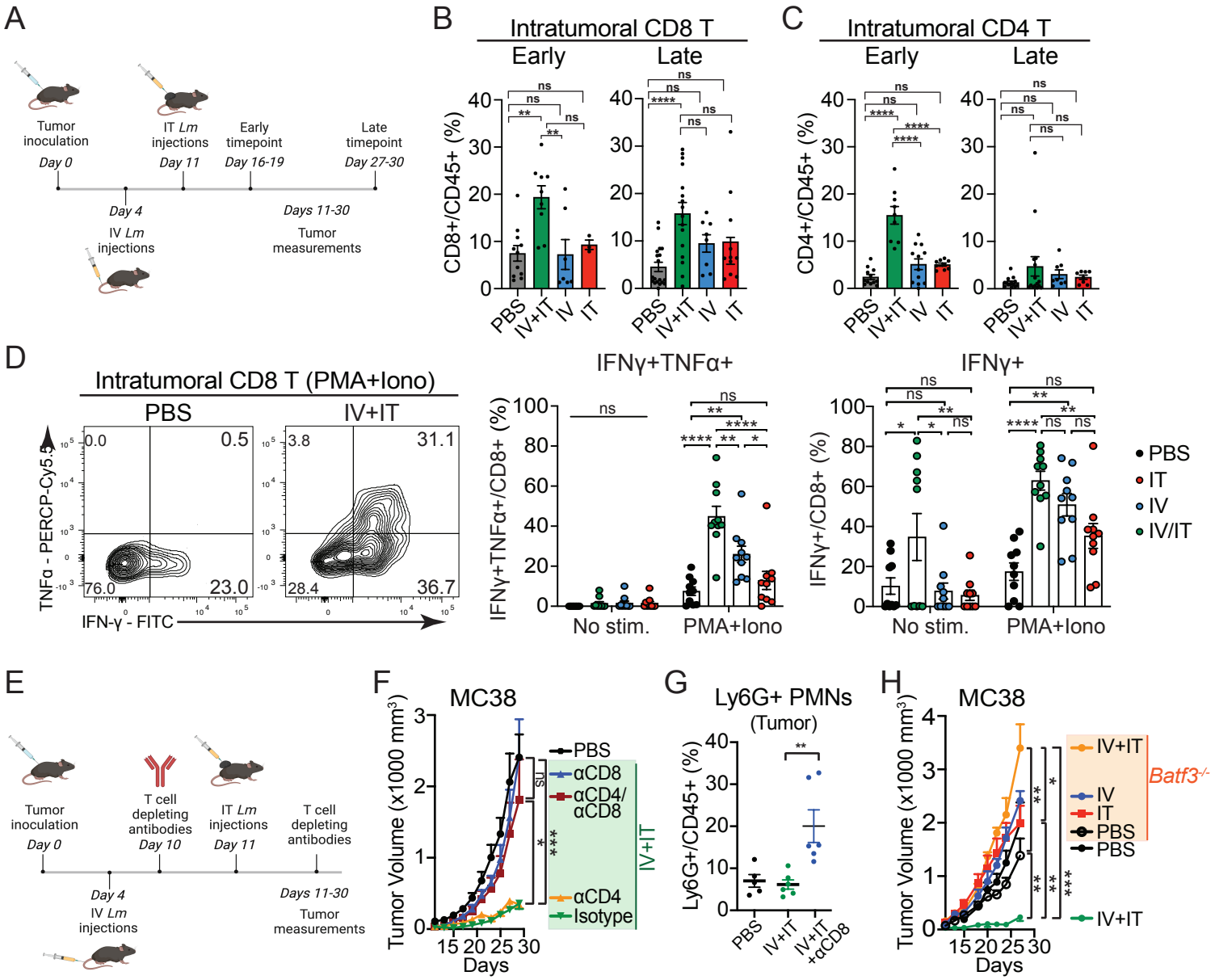
A
Tumor inoculation
Day 0
IT Lm injections
Day 11
Early timepoint
Day 16-19
Late timepoint
Day 27-30
Day 4
IV Lm injections
Days 11-30
Tumor measurements
B
Intratumoral CD8 T
Early
Late
CD8+/CD45+ (%)
PBS
IV+IT
IV
IT
C
Intratumoral CD4 T
CD4+/CD45+ (%)
D
Intratumoral CD8 T (PMA+Iono)
PBS
IV+IT
TNFα - PERCP-Cy5.5
IFN-γ - FITC
IFNγ+TNFα+
IFNγ+TNFα+/CD8+ (%)
No stim.
PMA+Iono
IFNγ+
IFNγ+/CD8+ (%)
PBS
IT
IV
IV/IT
E
Tumor inoculation
Day 0
T cell depleting antibodies
Day 10
IT Lm injections
Day 11
T cell depleting antibodies
Day 4
IV Lm injections
Days 11-30
Tumor measurements
F
MC38
Tumor Volume (x1000 mm³)
Days
PBS
αCD8
αCD4/αCD8
αCD4
Isotype
IV+IT
G
Ly6G+ PMNs
(Tumor)
Ly6G+/CD45+ (%)
PBS
IV+IT
IV+IT +αCD8
H
MC38
Tumor Volume (x1000 mm³)
Days
IV+IT
IV
IT
PBS
PBS
IV+IT
Batf3-/-

Figure 5 | $CD8^+$ T cells are required for tumor control with IV+IT *Lm*.
(A) Experimental strategy for IV+IT *Lm* dosing regimen followed by early or late flow cytometry analysis.
(B-C) Frequency of intratumoral $CD8^+$ (B) or $CD4^+$ (C) T cells of $CD45^+$ cells from MC38 tumors at early (left) or late (right) timepoints as specified in (A) (results pooled from four experiments with 5 mice/group).
(D) Representative flow plots for IFNγ and TNFα intracellular cytokine staining from intratumoral CD8 T cells 8 days after IT *Lm* or IT PBS administration in each *Lm* dosing regimen (results pooled from two experiments with 5 mice/group).
(E) Experimental strategy for IV+IT *Lm* dosing regimen plus anti-CD8, anti-CD4, or both depleting antibodies beginning 10 days after MC38 tumor inoculation.
(F) MC38 tumor growth with T cell depletion.
(G) Frequency of intratumoral $Ly6G^+$ PMNs of $CD45^+$ cells in IV+IT *Lm* treated mice +/- anti-CD8 depleting antibodies at end of experiment from (F).
(H) MC38 tumor growth in WT versus *Batf3*$^{-/-}$ mice treated with IV+IT *Lm*.
For all plots, *P<0.05, **P<0.01, ***P<0.001 by student t-test (B-C, G), one-way ANOVA (D), or two-way ANOVA (F, H), mean ± s.e.m.

Figure 6.

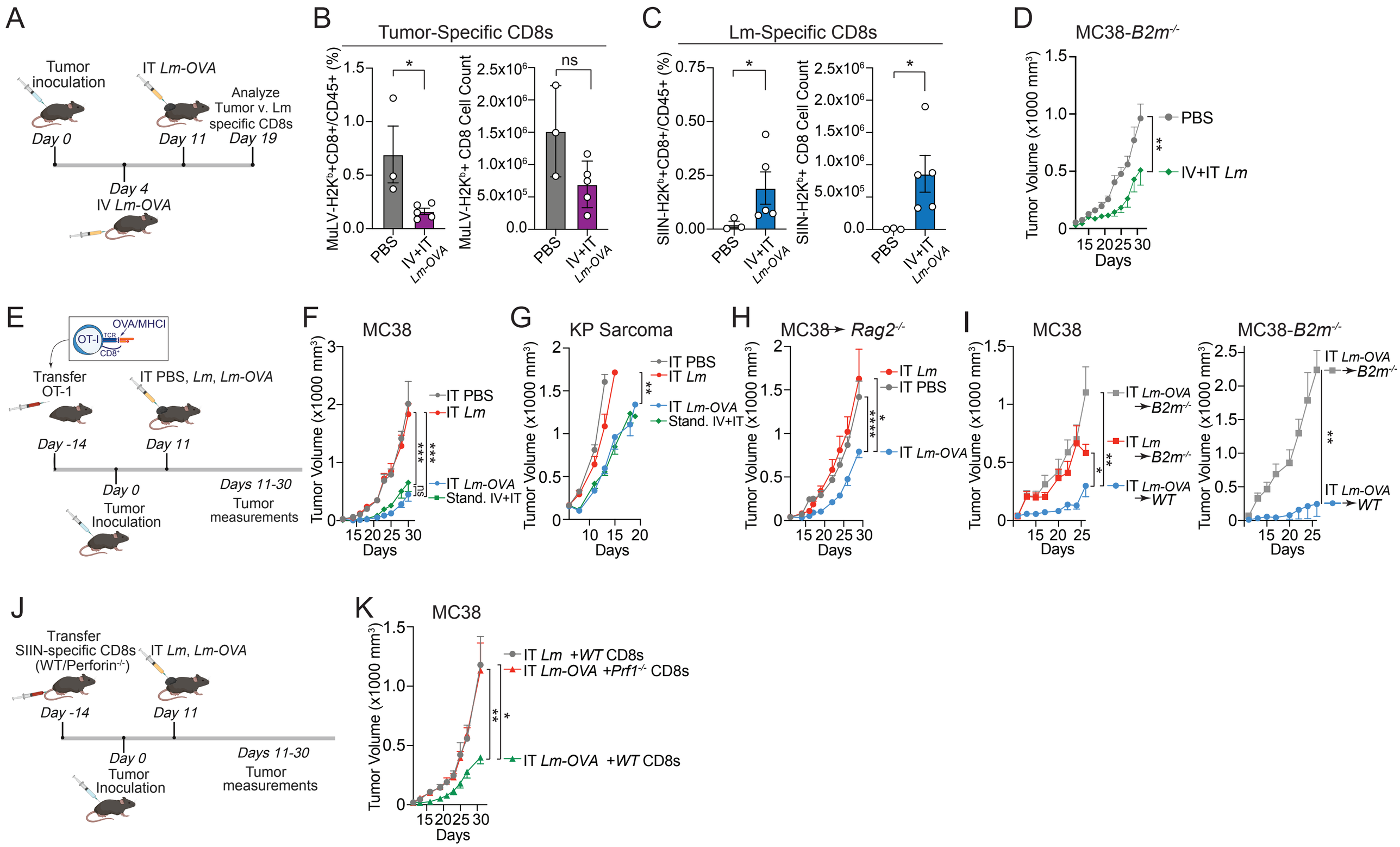
A
Tumor inoculation
IT Lm-OVA
Analyze Tumor v. Lm specific CD8s
Day 0
Day 11
Day 19
Day 4
IV Lm-OVA
B
Tumor-Specific CD8s
MuLV-H2Kᵇ+CD8+/CD45+ (%)
MuLV-H2Kᵇ+ CD8 Cell Count
PBS
IV+IT Lm-OVA
C
Lm-Specific CD8s
SIIN-H2Kᵇ+CD8+/CD45+ (%)
SIIN-H2Kᵇ+ CD8 Cell Count
D
MC38-B2m-/-
Tumor Volume (x1000 mm³)
Days
PBS
IV+IT Lm
E
OVA/MHCI
OT-I
TCR
CD8+
Transfer OT-1
IT PBS, Lm, Lm-OVA
Day -14
Day 11
Day 0
Tumor Inoculation
Days 11-30
Tumor measurements
F
MC38
IT PBS
IT Lm
IT Lm-OVA
Stand. IV+IT
G
KP Sarcoma
H
MC38→ Rag2-/-
I
MC38
MC38-B2m-/-
IT Lm-OVA →B2m-/-
IT Lm →B2m-/-
IT Lm-OVA →WT
J
Transfer SIIN-specific CD8s (WT/Perforin-/-)
IT Lm, Lm-OVA
K
IT Lm +WT CD8s
IT Lm-OVA +Prf1-/- CD8s
IT Lm-OVA +WT CD8s

Figure 6 | Anti-*Listeria* CD8 immunity mediates tumor control.
(A) Experimental design to analyze tumor-specific versus *Lm*-specific CD8 T cells after IV+IT *Lm*. OVA was expressed from *Lm* as a surrogate *Lm* antigen.
(B-C) Frequency (left) and total number (right) of tumor-specific (B, MuLV-H2K^b tetramer) and *Lm*-specific (C, SIIN-H2K^b tetramer) CD8 T cells from MC38 tumors 8 days after IT *Lm-OVA* in IV+IT *Lm-OVA* regimen.
(D) MC38-B2m$^{-/-}$ tumor growth after IV+IT *Lm* or IV+IT PBS.
(E) Experimental strategy to adoptively transfer *in vitro*-activated OT-I CD8 T cells in place of prophylactic IV *Lm.*
(F-I) OT-I CD8 T cells were adoptively transferred and MC38 tumors measured after IT PBS, *Lm*, or *Lm-OVA*.
(F) IT PBS, *Lm*, or *Lm-OVA* were compared against standard IV+IT without OT-I transfer (n= 5-6 mice/group from one of two experiments).
(G) As in (F) but using an orthotopic KP sarcoma model (n= 5-6 mice/group).
(H) As in (F) but in *Rag2*$^{-/-}$ mice (n= 5-6 mice/group).
(I) As in (F) but IT delivery compared MC38 tumors grown in WT or β2m$^{-/-}$ mice (left) or MC38-*B2m*$^{-/-}$ tumors grown in WT or β2m$^{-/-}$ mice (right) (n= 5-6 mice per group).
(J) Experimental strategy to adoptively transfer *in vitro* expanded SIIN-specific CD8 T cells from WT or *Prf1*$^{-/-}$ mice immunized with *Lm-OVA* (see methods).
(K) MC38 tumor growth after adoptive transfer of SIIN-specific CD8 T cells from WT or *Prf1*$^{-/-}$ mice followed by IT injection of PBS, *Lm*, or *Lm-OVA* at day 11 of tumor growth (n= 6 mice/group from one of two experiments).
For all plots, *P<0.05, **P<0.01, ***P<0.001 by student t-test (B, C) or or two-way ANOVA (D, F-H, I, K), mean ± s.e.m.